



Laporan Akhir Projek Penyelidikan Jangka Pendek

**Investigation Of Chitosan-SiO₂-
NH₄CH₃COO Membranes For Proton
Batteries Application**

by

Assoc. Prof. Dr. Ahmad Azmin Mohamad

Assoc. Prof. Dr. Zulkifli Mohamad Ariff

Siti Salwa Alias

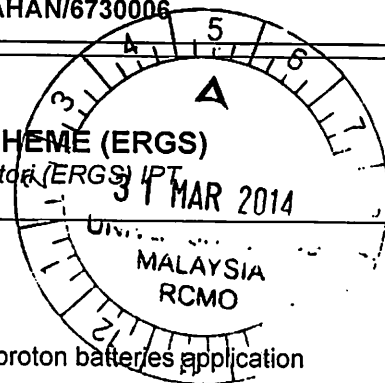
2014



KEMENTERIAN
PENDIDIKAN
MALAYSIA

FINAL REPORT
EXPLORATORY RESEARCH GRANT SCHEME (ERGS)

Laporan Akhir Skim Geran Penyelidikan Eksploratori (ERGS) IPT
2014



A PHASE : THIS PROJECT WAS COMPLETED
Fasa

RESEARCH TITLE : Investigation of chitosan-SiO₂-NH₄CH₃COO membranes for proton batteries application
Tajuk Penyelidikan

PROJECT LEADER : Assoc. Prof. Dr. Ahmad Azmin Mohamad
Ketua Projek

**PROJECT MEMBERS (including GRA) : 1. Assoc. Prof. Dr. Zulkifli Mohamad Ariff
2. Siti Salwa Alias (GRA)**
Ahli Projek

PROJECT ACHIEVEMENT (Prestasi Projek)

ACHIEVEMENT PERCENTAGE			
Project progress according to milestones achieved up to this period	0 - 50%	51 - 75%	76 - 100%
Percentage			100%
RESEARCH OUTPUT			
Number of articles/ manuscripts/ books (Please attach the First Page of Publication)	Refereed Journal	Non-Refereed Publication	
	1. N Alias, AA Mohamad Morphology Study for Electrodeposited Zinc from Zinc Sulfate Solutions as Anode for Aqueous Batteries, Journal of King Saud University-Engineering Sciences, 2013, in press. 2. MN Masri, MFM Nazari, CY Ng, AA Mohamad, Tapioca Binder for Porous Zinc Anodes Electrode in Zinc-Air Batteries, Journal of King Saud University-Engineering Sciences, 2013, in press. 3. Siti Salwa Alias; Siew Mian Chee; A.A. Mohamad, Chitosan-ammonium acetate-ethylene carbonate Membrane for Proton Batteries, Arabian Journal of Chemistry, 2014 minor correction.	[Book] Siti Salwa Alias Ahmad Azmin Mohamad, Synthesis of Zinc Oxide by Sol-Gel Method for Photoelectrochemical Cell, SpringerBriefs in Materials, 2014	

	International	National
Conference Proceeding (Please attach the First Page of Publication)	1. S. S. Alias and A. A. Mohamad. Preparation and Characterization of Porous Chitosan Membrane for Proton Battery. Proceeding International Conference on Materials for Advanced Technologies (ICMAT 2013), page 34. 2. Siti Salwa Alias, Zulkifli Mohamad Ariff, and Ahmad Azmin Mohamad. Preparation and Characterization of Porous Silica-Chitosan Membrane for Proton Batteries. Proceeding Asia-Pacific Conference on Electrochemical Energy Storage and Conversion (APEnergy2014).	

Intellectual Property
 (Including Paten, Copyright, Industrial Design, layout Design of Integrated Circuit & Trademarks)

HUMAN CAPITAL DEVELOPMENT

Human Capital	Number				Others (please specify)
	On-going		Graduated		
Citizen	Malaysian	Non Malaysian	Malaysian	Non Malaysian	
PhD Student	2		2		
Master Student	1		1		
Undergraduate Student					
Total	3		3		

EXPENDITURE (Perbelanjaan)

C Budget Approved (Peruntukan diluluskan) : RM 139,000
 Amount Spent (Jumlah Perbelanjaan) : RM 138,952
 Balance (Baki) : RM 48.00
 Percentage of Amount Spent : 100.00 %
 (Peratusan Belanja)

ADDITIONAL RESEARCH ACTIVITIES THAT CONTRIBUTE TOWARDS DEVELOPING SOFT AND HARD SKILLS
 (Aktiviti Penyelidikan Sampingan yang menyumbang kepada pembangunan kemahiran insaniah)

D	International		
	Activity	Date (Month, Year)	Organizer
	(e.g : Course/ Seminar/ Symposium/ Conference/ Workshop/ Site Visit)	-	-
	National		
	Activity	Date (Month, Year)	Organizer
	(e.g : Course/ Seminar/ Symposium/ Conference/ Workshop/ Site Visit)	Workshop on writing references using End Note and Mandaley. (12 NOVEMBER 2013)	Universiti Kuala Lumpur Malaysian Spanish Institute, Kulim Hi-TechPark, 09000 Kulim, Kedah.

PROBLEMS / CONSTRAINTS IF ANY (*Masalah/ Kekangan sekiranya ada*)

- E** Some problems that have been facing during preparation and characterization of the porous chitosan membranes:
- 1) The experimental method need to change to a few parameter in order to produce membranes with better structural properties.
 - 2) Due to some difficulties and instruments maintaining problems, the fabrication of proton batteries and analyses process need to delayed several times.
 - 3) The process of review paper after submitted to journals take a lots of time.

RECOMMENDATION (*Cadangan Penambahbaikan*)

F It suggested that future research work should focus on producing porous chitosan membrane using other simple technique such as ultrasonicator. This is because this technique will reduce the duration of sample preparation besides can produce uniform pore size and shape.

Other kind of salt such as ammonium nitrate, ammonium bromide can be used to replace ammonium acetate. Different kind of salts can give various results in term of electrochemical properties. Besides that, all the electrochemical properties can be investigated at high temperature. The analysis of fabricated proton batteries can be focus on elevated temperatures to find the resistance of batteries besides focus on failure analysis of batteries.

RESEARCH ABSTRACT – Not More Than 200 Words (Abstrak Penyelidikan – Tidak Melebihi 200 patah perkataan)

G The porous chitosan acetate-silica membranes were prepared using inverse porogen/polymer solubility technique. Different concentration of sodium hydroxide porogen removal solution was used to dissolve silica from chitosan acetate membrane. The optimum chitosan to silica ratio for producing largest macroporous membrane was 1:4. The morphology and structural properties showed optimum average pore size and degree of crystallinity of 5.9 μm and 90%, respectively. Fourier transform infrared analysis showed the interaction between chitosan, acetic acid and silica have been occurred based on the shifting of several functional group peaks intensity. The melting point of the membrane obtained from differential scanning calorimetry was 130°C. Thermogravimetry analysis shows the decomposition of the total of the membrane begins at a temperature of 200°C. The membrane had the higher conductivity of $(4.7 \pm 1.1) \times 10^{-2} \text{ S cm}^{-1}$ after two-day immersion in 5.0 M ammonium acetate electrolyte solution compared with the membrane before immersed in ammonium acetate electrolyte $(6.0 \pm 0.1) \times 10^{-8} \text{ S cm}^{-1}$. Fabricated proton batteries displayed an open circuit potential of 1.5 V for 8 days and turned on LED for 40 hours. The internal current resistance of batteries was 0.02 Ω and maximum power density of 11.0 mW cm^{-2} . The specific discharge capacities of proton batteries were 6.4, 10.7, 35.6 and 53.3 mA h g^{-1} for 0.1, 0.2, 0.5 and 1.0 mA discharge current, respectively.

Date : 26/3/14
Tarikh

Project Leader's Signature:
Tandatangan Ketua Projek

AHMAD AZMIN MOHAMAD
B.Sc. Hons (Malaya), Ph.D. (Malaya)
Associate Professor

COMMENTS, IF ANY/ ENDORSEMENT BY RESEARCH MANAGEMENT CENTER (RMC)
(Komen, sekiranya ada/ Pengesahan oleh Pusat Pengurusan Penyelidikan)

School of Materials & Mineral Resources Engineering,
Universiti Sains Malaysia,
14300 Nibong Tebal, Penang, Malaysia.
E-mail: azmin@eng.usm.my

H

Good outputs

Name:
Nama:

PROF. MADYA LEE KEAT TEONG
Pengarah
Pejabat Pengurusan & Kreativiti Penyelidikan
Universiti Sains Malaysia
11800 USM, Pulau Pinang.

Signature:
Tandatangan:



Date:
Tarikh:

1/4/14

Tajuk Projek : INVESTIGATION OF CHITOSAN-NH4NO3-EC-GA MEMBRANES FOR PROTON
 BATTERIES APPLICATION
 PROFESOR MADYA AHMAD AZMIN MOHAMAD
 Pusat Pengajian : Pusat Pengajian Kejuruteraan Bahan dan Sumber Mineral
 Penyelidik : AHMAD AZMIN MOHAMAD

Status Projek : AKTIF

No Projek (Agensi) :

Tempoh Projek : 2011 / 8 - 2014 / 3

No Akaun : 203 / 6730006

<u>Vot</u>	<u>Keterangan</u>	<u>Peruntukan Asal</u> (a)	<u>Perbelanjaan Tahun Lalu</u> (b)	<u>Peruntukan Semasa</u> (c)	<u>Tanggungjawab</u> (d)	<u>Belanja</u> (e)	<u>Jumlah Belanja</u> (f) = (d) + (e)	<u>Baki</u> (a) - (f)	<u>%</u> ((b)+(f)) / (a)
11000	Gaji	40,000.00	\$25,699.49	\$0.00	\$0.00	\$0.00	\$0.00	\$14,300.51	0.00
		\$40,000.00	\$25,699.49	0.00	\$0.00	\$0.00	\$0.00	\$14,300.51	0.00
21000	PERJALANAN DAN SARA HIDUP	14,000.00	\$8,546.35	\$0.00	\$720.00	\$0.00	\$720.00	\$4,733.65	0.00
23000	PERHUBUNGAN DAN UTILITI	200.00	\$1,200.00	\$0.00	\$0.00	\$0.00	\$0.00	(\$1,000.00)	0.00
27000	BEKALAN DAN ALAT PAKAI HABIS	58,800.00	\$43,043.95	\$0.00	\$6,383.70	\$0.00	\$6,383.70	\$9,372.35	0.00
28000	PENYELENGGARAAN DAN PEMBAIKAN KECIL	0.00	\$100.00	\$0.00	\$0.00	\$0.00	\$0.00	(\$100.00)	0.00
29000	PERKHIDMATAN IKTISAS DAN HOSPITALITI	1,000.00	\$23,615.88	\$0.00	\$2,278.82	\$2,743.00	\$5,021.82	(\$27,637.70)	0.00
		\$74,000.00	\$76,506.18	0.00	\$9,382.52	\$2,743.00	\$12,125.52	(\$14,631.70)	0.00
35000	HARTA-HARTA MODAL LAIN	25,000.00	\$22,600.00	\$0.00	\$0.00	\$1,200.00	\$1,200.00	\$1,200.00	0.00
		\$25,000.00	\$22,600.00	0.00	\$0.00	\$1,200.00	\$1,200.00	\$1,200.00	0.00
		\$139,000.00	\$124,805.67	\$0.00	\$9,382.52	\$3,943.00	\$13,325.52	\$868.81	0.00

**FINAL REPORT OF EXPLORATORY
RESEARCH GRANT SCHEME
(ERGS)**

**Investigation of Porous
Chitosan-SiO₂-NH₄CH₃COO Membranes for
Proton Batteries Application
(203/PBAHAN/6730006)**

PROJECT LEADER: Assoc. Prof. Dr. Ahmad Azmin Bin Mohamad

**PROJECT MEMBERS: 1. Assoc. Prof. Dr. Zulkifli Mohamad Ariff
(including GRA) 2. Siti Salwa Binti Alias**

ABSTRACT

This project is divided into three sections: the preparation of porous chitosan acetate-silica membranes in a range of $\sim 6.0 \mu\text{m}$ pores size with good morphological, structural and thermal properties; improvement the conductivity of porous chitosan acetate-silica-ammonium acetate membranes up to $10^{-2} \text{ S cm}^{-1}$; and fabrication of $\text{Zn}+\text{ZnSO}_4 \cdot 7\text{H}_2\text{O}$ /porous chitosan acetate-silica-acetate membranes/ MnO_2 coin cell to improve the battery specific capacity up to 55.0 mA h g^{-1} . The porous chitosan acetate-silica membranes were prepared using inverse porogen/polymer solubility technique. Different concentration of sodium hydroxide porogen removal solution was used to dissolve silica from chitosan acetate membrane. The optimum chitosan to silica ratio for producing largest macroporous membrane was 1:4. The morphology and structural properties showed optimum average pore size and degree of crystallinity of $5.9 \mu\text{m}$ and 90%, respectively. Fourier transform infrared analysis showed the interaction between chitosan, acetic acid and silica have been occurred based on the shifting of several functional group peaks intensity. The melting point of the membrane obtained from differential scanning calorimetry was 130°C . Thermogravimetry analysis shows the decomposition of the total of the membrane begins at a temperature of 200°C . The membrane had the higher conductivity of $(4.7 \pm 1.1) \times 10^{-2} \text{ S cm}^{-1}$ after two-day immersion in 5.0 M ammonium acetate electrolyte solution compared with the membrane before immersed in ammonium acetate electrolyte $(6.0 \pm 0.1) \times 10^{-8} \text{ S cm}^{-1}$. Fabricated proton batteries displayed an open circuit potential of 1.5 V for 8 days and turned on LED for 40 hours. The internal current resistance of batteries was 0.02Ω and maximum power density of 11.0 mW cm^{-2} . The specific discharge capacities of proton batteries were 6.4, 10.7, 35.6 and 53.3 mA h g^{-1} for 0.1, 0.2, 0.5 and 1.0 mA discharge current, respectively.

ABSTRAK

Projek ini terbahagi kepada tiga bahagian: penyediaan membran kitosan asetat-silika berliang dalam julat saiz liang $\sim 6.0 \mu\text{m}$; peningkatan kekonduksian berliang kitosan membran asetat-silika-ammonium asetat sehingga $10^{-2} \text{ S cm}^{-1}$ dengan ciri morfologi, struktur dan terma yang baik; dan fabrikasi $\text{Zn}+\text{ZnSO}_4 \cdot 7\text{H}_2\text{O}$ /membran kitosan asetat-silika berliang/ MnO_2 sel syiling dengan peningkatan kapasiti tertentu bateri sehingga 55.0 mA h g^{-1} . Membran kitosan asetat-silika berliang disediakan dengan menggunakan teknik songsang porogen/kelarutan polimer. Sodium hidroksida dengan kepekatan yang berbeza digunakan untuk mengeluarkan silika dari membran kitosan asetat-silika berliang. Nisbah kuantiti terbaik serbuk kitosan kepada nisbah silica ialah 1:4. Analisis morfologi dan struktur menunjukkan purata saiz liang terbesar dan darjah penghabluran bagi membran adalah $5.9 \mu\text{m}$ dan 90 %, masing-masing diperolehi. Analisis inframerah transformasi Fourier menunjukkan interaksi antara chitosan, asid asetik dan silika telah berlaku berdasarkan peralihan keamatan beberapa puncak kumpulan berfungsi. Takat lebur bagi membran yang diperolehi dari kalorimetri pengimbasan pembezaan adalah 130°C . Ujian termogravimetri menunjukkan penguraian total bagi membran bermula pada suhu 200°C . Membran yang direndam selama dua hari di dalam larutan elektrolit ammonium asetat berkepekatan 5.0 M mempunyai kekonduksian yang lebih tinggi iaitu $(4.7 \pm 1.1) \times 10^{-2} \text{ S cm}^{-1}$ berbanding membran sebelum direndam dalam 5.0 M larutan elektrolit ammonium asetat $(6.0 \pm 0.1) \times 10^{-8} \text{ S cm}^{-1}$. Bateri proton yang difabrikasi menunjukkan potensi litar terbuka 1.5 V selama 8 hari dan boleh menghidupkan diod pemancar cahaya selama 40 jam. Rintangan dalam bateri adalah 0.02Ω dan ketumpatan kuasa maksimum 11.0 mW cm^{-2} . Kapasiti tertentu proton bateri proton adalah 6.4, 10.7, 35.6 dan 53.3 mA h g^{-1} untuk arus nyahcas 0.1, 0.2, 0.5 dan 1.0 mA.

CHAPTER 1

INTRODUCTION

1.1 Battery and Its Components

A battery is a device which converts the energy liberated in a chemical reaction into electricity. The main functions of a battery are to act as portable sources of electric power as well as to store electrical energy supplied by an external source. A typical battery consists of a cathode, an anode and the electrolyte. The cathode is connected to the negative terminal while the anode is connected to the positive terminal. The electrolyte contains ions which react with the electrodes to generate chemical energy.

In general, there are two types of batteries-primary and secondary batteries. A primary battery has a life which only lasts until all the reactants have been consumed by the discharge process. On the other hand, secondary batteries can be charged or recharged and may be considered as an electrochemical storage unit. The cell may be restored to its original charged condition by applying current in the opposite direction to that of discharge. Due to this nature, secondary batteries are also known as rechargeable batteries (Vincent and Scrosati, 1997).

The first practical rechargeable battery invented was a lead-acid battery in 1859. This battery system is still being used extensively today as engine starting (starting, lighting and ignition, SLI) and stationary emergency power. Another well established rechargeable battery system is the nickel-cadmium (Ni-Cd) system which is used in portable tools, instruments, military and aerospace equipments. Other battery systems in commercial use today include nickel-metal hydride (Ni-MH), zinc-

manganese dioxide (Zn-MnO₂) and lithium (Li⁺) ion batteries (Beck and Rüetschi, 2000).

Rüetschi proposed the “three E” criteria (energy, economics and environment) for determining the success of a battery system. In terms of energy, the battery should have high energy content with respect to unit weight and volume. Economics simply refer to low manufacturing costs, low maintenance during use and long service life. Lastly, environment means that the battery is free from toxic materials, safe, has low energy consumption during manufacture and use, has high reliability and is easy to recycle (Beck and Rüetschi, 2000).

The three criteria lead to rapid development of non-toxic, biodegradable and cheap materials for battery components especially in terms of solid state electrolytes. For example, chitosan is a naturally available and abundant biopolymer which has potential as a polymer host for ammonium salts in a polymer electrolyte (Ng and Mohamad, 2006). Ammonium acetate (CH₃COONH₄) also provides a cheap and safe choice of ammonium salt to be complexed with chitosan (Du et al., 2009).

While the term “battery” is often used, the basic electrochemical unit being referred to is the “cell”. A cell provides a source of electric energy by direct conversion of chemical energy. The cell consists of an assembly of electrodes, separator, electrolyte, container and terminals. A battery consists of one or more of these cells, connected in series or parallel, or both, depending on the desired output voltage and capacity. Figure 1.1 shows an example of the cell components. The cell consists of three major components (Linden, 2002):

- i. The anode or negative electrode – the reducing or fuel electrode, which gives up electrons to the external circuit and is oxidized during the electrochemical reaction.

- ii. The cathode or positive electrode – the oxidizing electrode, which accepts electrons from the external circuit and is reduced during the electrochemical reaction.
- iii. The electrolyte or the ionic conductor – which provide the medium for transfer of charge, as ions, inside the cell between the anode and cathode. The electrolyte is typically a liquid (water or alcohols solvents), with dissolved salts, acids or alkalis to impart ionic conductivity. Nowadays, some batteries use solid electrolytes.

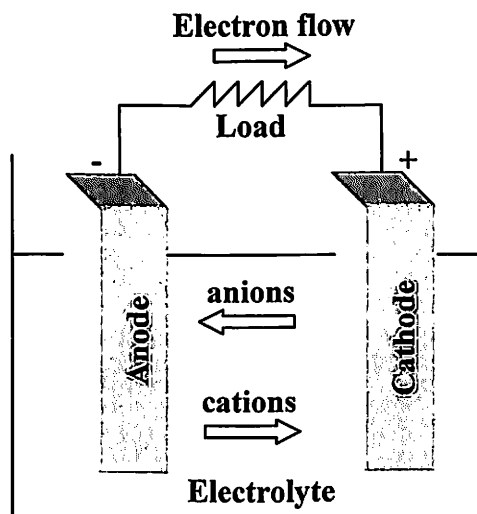


Figure 1.1: The cell components (discharge operation) (Linden, 2002).

A significant characteristic of a protonic battery is that charging/discharging can be done by shifting protons (H^+) (NEC TOKIN, 2004). The source of H^+ is from electrolyte. The electrolyte can be prepared either in liquid, gel or solid-state form. For a successful protonic battery, an anode capable of supplying or injecting H^+ ions into the battery electrolyte, a proton conducting electrolyte and a reversible cathode with layered oxides are needed (Pratap et al., 2006). In protonic battery, zinc (Zn)

and manganese (IV) oxide (MnO_2) have been used as anode and cathode material, respectively. The optimum concentration of electrolyte will provide highest mobility of H^+ ions. Consequently the conductivity of electrolyte can be enhanced.

1.2 Solid State Electrolyte

Solid materials which are capable of ionic conduction have many advantages over their liquid equivalents. This is especially true in preventing leakage of harmful liquids and the potential of producing miniaturized cells. Some of the solid state electrolyte systems are crystalline solid electrolyte, glass electrolyte and polymer electrolyte (Gray, 1997).

Crystalline solid electrolytes can conduct cations and anions. High concentration of mobile ions and a low activation energy for ionic motion from site to site result in high ionic conductivity. The number of sites available for mobile ions is much greater than the number of mobile ions present. This leads to high diffusion coefficients and fast ion conductors. According to Gray (1997), many researches on crystalline solid electrolytes revolve around sodium ion (Na^+) conduction owing to the well-studied sodium β -aluminas and Na superionic conductors (NASICON) systems.

Glasses can also transport ions. Glass electrolyte systems have a more complex composition. But in general, the composition consists of three basic constituents which are the network formers, network modifiers and ionic salts. Network formers such as silica (SiO_2) and phosphorus pentasulfide (P_2S_5) form the crosslinked macromolecular chains. Network modifiers interact with the network former structure by breaking the oxygen and sulfide bridges to introduce ionic bonds. Oxides and sulfides such as silver oxide (Ag_2O) and lithium sulfide (Li_2S) are

network modifiers. The ionic salts do not react chemically with the macromolecular structure but increases the ionic conductivity (Gray, 1997).

Polymer electrolyte is generally known as a solvent-free system where the ionically conducting phase is formed by complexing salts with a high molecular weight polymer matrix. Some of the polymers researched as proton conducting material include polyethylene oxide (PEO), poly(vinyl alcohol) (PVA) and chitosan (Ng and Mohamad, 2008). Interestingly, when Gray (1997) compared crystalline solid and glass electrolytes to polymer electrolyte, the crystalline solid and glass electrolytes are at a disadvantage due to their hard and brittle nature. In contrast, polymer electrolytes have form flexibility which allows good interfacial contact with the electrodes.

1.3 Problem Statement

Ceramic fillers such as silica (SiO_2), alumina (Al_2O_3), copper oxide (CuO) or titanium oxide (TiO_2) particles have been used to enhance morphology, structural and electrical properties of polymer electrolyte (Kim et al., 2002; Liu et al., 2003; Li et al., 2005; Kim et al., 2006). Among of these fillers, SiO_2 has excellent properties to produce porous membrane (Zeng and Ruckenstein, 1996; Kim et al., 2001; Kim et al., 2006; Santos et al., 2008). It has been widely utilized in various application such as dehumidification processes (Chang et al., 2004), medical purpose (Vallet-Regi et al., 2006) and electrochemical sensors (Wang et al., 2009). However, the application limited only for rechargeable lithium battery (Kim et al., 2001; Kim et al., 2006).

Normally, SiO_2 particles are insoluble in acidic media but soluble in alkaline sodium hydroxide (NaOH) solutions (Zeng and Ruckenstein, 1996; Santos et al., 2008). The extraction of SiO_2 particles after immersed in NaOH can generate porous

chitosan membrane. The large pore size of chitosan membrane is somewhat important in solid polymer electrolyte requirement. The combination of porous chitosan membrane with good salts will allow more chelation of proton (H^+) compared to the dense membrane. This can produce batteries with good properties. However, the previous studies only focused on one concentration of NaOH solution such as 8.0 wt. % (Clasen et al., 2006), 1.0 M (Mei et al., 2012), 0.067 M (Zeng and Ruckenstein, 1996) and 0.25 M (Shirosaki et al., 2005) instead of vary NaOH in different concentration to remove SiO_2 particles.

1.4 Objectives

The main objectives of this project are:

- a) To prepare of porous chitosan acetate-silica membranes in a range of ~ 6.0 μm pores size with good morphological, structural and thermal properties.
- b) To improve the conductivity of porous chitosan acetate-silica-ammonium acetate membranes up to $10^{-2} S cm^{-1}$.
- c) To fabricate $Zn+ZnSO_4 \cdot 7H_2O$ /porous chitosan acetate-silica-acetate membranes/ MnO_2 coin cell and improve the battery specific capacity up to $55.0 mA h g^{-1}$.

1.5 Approach of Study

The porous chitosan acetate membrane (CA) was prepared using the stirring mixed solution-cast method by applying SiO_2 as porogen agent. After that, SiO_2 particles were dissolved in NaOH at different concentration. Then, the porous SiO_2 -CA membrane with optimal morphological, structural and thermal properties was immersed in the NH_4CH_3COO electrolyte solution. Finally, the porous SiO_2 -CA-

$\text{NH}_4\text{CH}_3\text{COO}$ membrane was used to fabricate proton batteries. The proton batteries open circuit potential (OCP), discharge profile, current-voltage (I - V), and current density-power density (J - P) characteristics were investigated in this studies.

CHAPTER 2

EXPERIMENTAL PROCEDURE

2.1 Introduction

This chapter explains the experimental materials, methodologies, and testing instruments. Various kinds of testings have been performed in order to obtain the best results from the proposed methodologies. This chapter is made up of three parts including:

- a) Preparation and characterization of porous chitosan acetate-silica membranes using inverse porogen/polymer solubility technique.
- b) Immersion of porous chitosan acetate-silica membrane in ammonium acetate ($\text{NH}_4\text{CH}_3\text{COO}$) solution electrolyte and electrochemical analysis of membrane.
- c) Fabrication and characterization of $\text{Zn}+\text{ZnSO}_4\cdot 7\text{H}_2\text{O}$ /porous chitosan acetate-silica-ammonium acetate membranes/ MnO_2 proton battery coin cell.

2.2 Materials

2.2.1 Porous membrane and electrolyte materials

- a) Chitosan powder (Chito-Chem)
- b) High-purity grade silica gel, (60 Å pore size and 5 µm to 25 µm particle size; Sigma–Aldrich)
- c) Acetic acid (CH₃COOH, 99-100%, Merck)
- d) Sodium hydroxide (NaOH, Merck)
- e) Ammonium acetate (CH₃COONH₄, Merck)
- f) Glycerol (C₃H₅(OH)₃, 85%, Merck)

2.2.2 Proton Battery materials

- a) Zinc powder (Zn, Merck)
- b) Acetylene black (AB, Gunbai)
- c) Polytetrafluoroethylene (PTFE, Fluka)
- d) Manganese dioxide (MnO₂, Battery grade, Aldrich)
- e) Nickel mesh
- f) Coin cell

2.3 Porous CA-SiO₂: preparation and characterization

Chitosan acetate (CA) membranes were prepared using stirring and solution-cast technique. Chitosan powder (1.0 g; Aldrich) was dissolved in 1% acetic acid solution (CH₃COOH, Merck). The CA mixture was stirred continuously at 25 °C for 1 d using magnetic stirrer.

High-purity grade silica (SiO₂, 60 Å pore size and 5 µm to 25 µm particle size; Sigma-Aldrich) were dispersed with chitosan/SiO₂ weight ratio 1:4 into the CA

solution. The CA-SiO₂ solutions were then stirred for 1 day. The solutions were further dispersed using sonicator for 30 min. After complete dispersion of SiO₂, the solutions were placed into Petri dishes and left to dry at 25 °C to obtain CA-SiO₂ membranes.

Next, the CA-SiO₂ membranes were immersed in different concentration of NaOH (Merck) from 1.3, 3.0, 5.0 and 8.0 M at 60 °C for 1 d to dissolve SiO₂ particles from the membrane. The porous CA-SiO₂ membranes were washed with deionized water at first. The porous membranes were then plasticized by immersion in 2.2 M glycerol (Merck) for 30 min. Subsequently, the porous CA-SiO₂ membranes were washed with deionized water and allowed to dry at 25 °C. Membranes compositions were coded as tabulated in Table 2.1. Figure 2.1 illustrates the process preparation of porous CA-SiO₂ using inverse porogen/polymer solubility technique.

Table 2.1: Membranes codes based on CA-SiO₂-NaOH composition.

Sample name	Chitosan (g)	SiO ₂ (g)	NaOH (M)
Chitosan powder	-	-	-
Chitosan acetate (CA)	1	-	-
CA4S	1	4	-
CA4S 1.3N	1	4	1.3
CA4S 3.0N	1	4	3.0
CA4S 5.0N	1	4	5.0
CA4S 8.0N	1	4	8.0

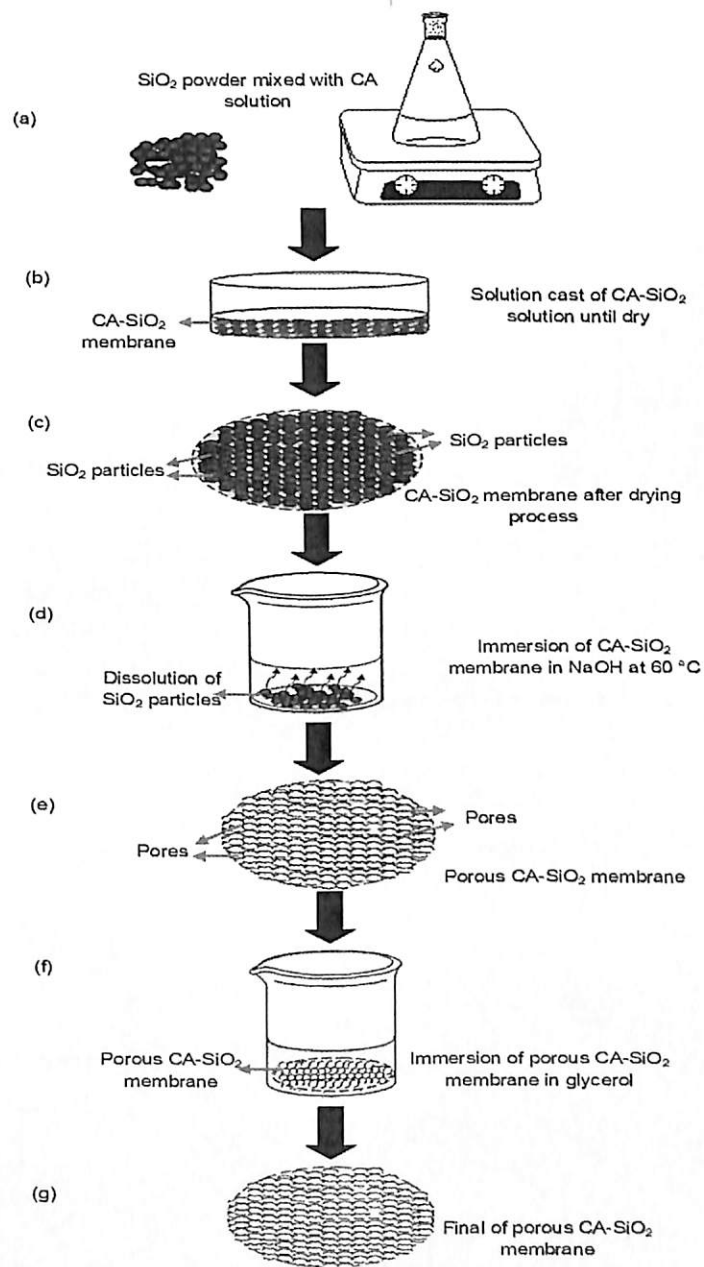


Figure 2.1: Preparation of porous CA-SiO₂ using inverse porogen/polymer solubility technique.

The morphology and composition of the porous CA-SiO₂ membranes was investigated using field emission scanning electron microscopy (FESEM) and energy dispersive X-ray spectroscopy (EDX, Zeiss Supra 35VP). Average pore sizes were calculated using Image J software. Structural properties were examined using X-ray diffraction (XRD; Bruker Advanced X-ray Solutions D8). Deconvolution of XRD

and degree of crystallinity of porous CA-SiO₂ membranes were further analyzed using Origin 8 software.

The thermal analysis of membrane were carried out using differential scanning calorimetric (DSC, Perkin Elmer DSC-6) and thermogravimetric analysis (TGA, Perkin Elmer Pyris 6 TGA analyzer). The DSC was used to determined the melting characterization of membranes. The heating and cooling rate was set at 10°C/min from 30-200°C. The samples were held at that temperature for 1 minute to eliminate thermal history, then the non isothermal crystallization process was recorded from 200-30°C. Meanwhile, TGA analysis was scanned from 30-600°C in a nitrogen flow of 30ml/min with heating rate 20°C/min.

2.4 Porous CA-SiO₂-NH₄CH₃COO: preparation and characterization

The electrolyte solution was prepared by dissolving different concentration of ammonium acetate (NH₄CH₃COO, Merck) from 1.0-7.0 M in deionized water. The amount NH₄CH₃COO of is tabulated in Table 2.2.

Next, electrochemical impedance spectroscopy (EIS) was used to measure the conductivity of NH₄CH₃COO electrolyte at room temperature using the Autolab PGSTAT 30 Frequency Response Analyzer (Eco Chemie B.V.) and frequency response analyzer (FRA) was set with frequency range of 0.1 Hz to 1.0 MHz and amplitude of 10 mV. The conductivity of an electrolyte can be calculated from the bulk resistance value (R_b) using the Equation 2.1:

$$\sigma = \frac{t}{R_b A} \quad (2.1)$$

where σ is the conductivity of electrolyte, t , thickness of sample = 0.41 cm, and A is the area of sample in teflon ring = 2.08 cm². This plot is also known as the Nyquist plot.

Table 2.2: Details of conductivity test sample for NH₄CH₃COO.

Sample name	Concentration (M)	Weight (g)
Deionized water	-	-
1.0AA	1.0	1.54
3.0AA	3.0	4.62
5.0AA	5.0	7.71
7.0AA	7.0	10.79

After that, the porous CA-SiO₂ membrane with largest average size of pores obtained from Section 2.1 was immersed in the highest conductivity of NH₄CH₃COO electrolyte for 2 days. Later, the conductivity of porous CA-SiO₂-NH₄CH₃COO electrolyte was measured using EIS compared with the conductivity of porous CA-SiO₂ before immersed in NH₄CH₃COO electrolyte. The conductivity of both samples can be calculated from R_b using the Equation 2.1. This electrolyte provided proton (H⁺) as a source for porous CA-SiO₂ membranes.

Both of these samples (porous CA-SiO₂-NH₄CH₃COO and porous CA-SiO₂ membranes) were chosen for conductivity measurement at elevated temperature from 25 to 90°C as shown in Figure 2.2.

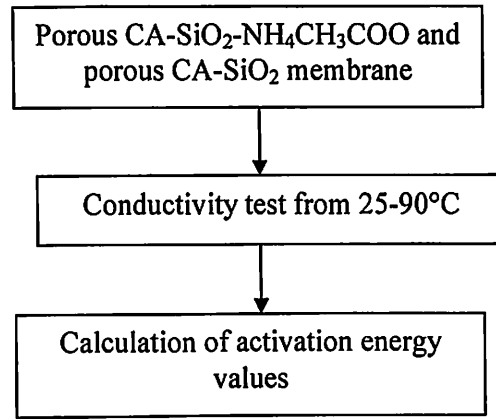


Figure 2.2: Preparation of samples for conductivity test at elevated temperature.

The Arrhenius plot (graph of $1000/T$ versus \log conductivity) were then plotted for both samples. The activation energy values of samples were then calculated based on this graph by using derivation of Equation 2.2-2.8 (Chang, 1998):

$$\sigma = \sigma_0 e^{\frac{-E_a}{kT}} \quad (2.2)$$

$$\ln \sigma = \ln \sigma_0 e^{\frac{-E_a}{kT}} \quad (2.3)$$

$$\ln \sigma = \ln \sigma_0 - \frac{E_a}{kT} \quad (2.4)$$

$$\ln \left(\frac{\sigma}{\sigma_0} \right) = -\frac{E_a}{kT} \quad (2.5)$$

Since $\ln x = 2.303 \log x$, hence Equation. 2.5 become:-

$$2.303 \log \frac{\sigma}{\sigma_0} = -\frac{E_a}{kT} \quad (2.6)$$

$$\log \sigma = \left(\frac{-E_a}{2.303k} \right) \left(\frac{1}{T} \right) + \log \sigma_0 \quad (2.7)$$

where σ is conductivity at 25°C, σ_0 is the pre exponential factor, k is the Boltzmann constant (8.62×10^{-5} eV K⁻¹), and T is the absolute temperature in Kelvin (273 K). Equation 2.8 can be rearranged to a linear equation:

$$\log \sigma = \left(\frac{-E_a}{2.303k} \right) \left(\frac{1}{T} \right) + \log \sigma_0 \quad (2.8)$$

$$\begin{array}{ccccccc} \updownarrow & & \updownarrow & & \updownarrow & & \updownarrow \\ y & & m & & x & + & c \end{array}$$

Since a plot of $1000/T$ versus \log conductivity gives a straight line whose slope m is equal to $E_a/2.303k$ and intercept c with the ordinate of Y-axis is $\log \sigma_0$, the values of activation energy were then calculated from $E_a/2.303k$ equal to m .

Linear sweep voltammetry (LSV) for porous CA-SiO₂-NH₄CH₃COO and porous CA-SiO₂ membrane were measured at from 0.0-2.0 V with scan rate of 0.01 V s⁻¹. Meanwhile cyclic voltammetry (CV) was measure from 0.3-3.0 V with scan rate 0.05 V s⁻¹. Both of this analysis were measured using Autolab PGSTAT 30 (Eco Chemie B.V.) with NOVA 1.9 software.

2.5 Porous CA-SiO₂-NH₄CH₃COO membrane proton batteries

Proton batteries coin cells were fabricated using the porous CA-SiO₂-NH₄CH₃COO membrane electrolyte in Section 2.4. The anode pellet was prepared with a mixture of Zn powder (particle size <45 μm; Merck), ZnSO₄·7H₂O powder (Univar), Super P powder (specific surface area of 62 m² g⁻¹; TIMCAL Graphite & Carbon), and polytetrafluoroethylene (PTFE, Fluka). The cathode pellet was prepared with a mixture of MnO₂ (Aldrich), Super P powder, and PTFE. The current collector, stainless steel mesh (area = 1.8 cm²), was placed in the middle of both pellets. All materials were combined and fabricated as Zn+ZnSO₄·7H₂O + Super P +

PTFE || CA-SiO₂-NH₄CH₃COO || MnO₂ + Super P + PTFE proton battery. The schematic diagram of coin cell proton battery illustrated in Figure 2.3.

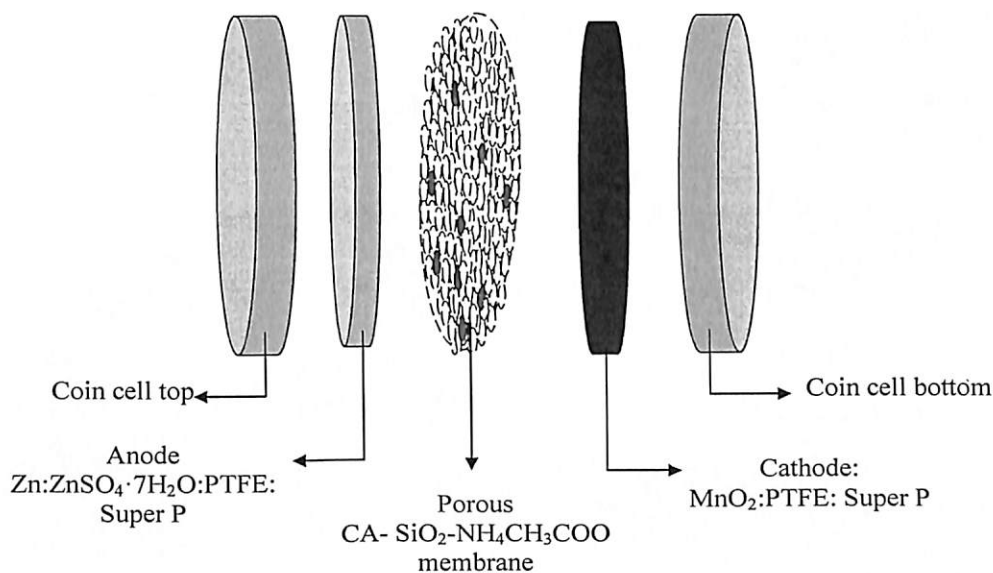


Figure 2.3: Schematic diagram of proton battery coin cell.

Neware BTS was used to characterize the open circuit potential (OCP) and discharge profile at 0.1, 0.2, 0.5 and 1.0 mA of proton batteries. The current voltage ($I-V$) and current density-power density ($J-P$) curves were plotted using a discharge current ranging from 20 μ A to 100 mA. The average voltage of both batteries was monitored for each current drain after a 10 s operation. This analysis was done using were measured using the galvanostat of Autolab PGSTAT 30 GPES (Eco Chemie B.V.). Figure 2.4 shows the fabrication and characterization test of Zn+ZnSO₄·7H₂O + Super P + PTFE || CA- SiO₂-NH₄CH₃COO || MnO₂ + Super P + PTFE proton battery. The battery was simulated via MULTISIM 11 to ensure that they can operate same with actual applications. All input values were given based on the OCV, discharge profile, and $I-V$ plot results. Afterward, the simulation was compared with the actual performance of the fabricated batteries.

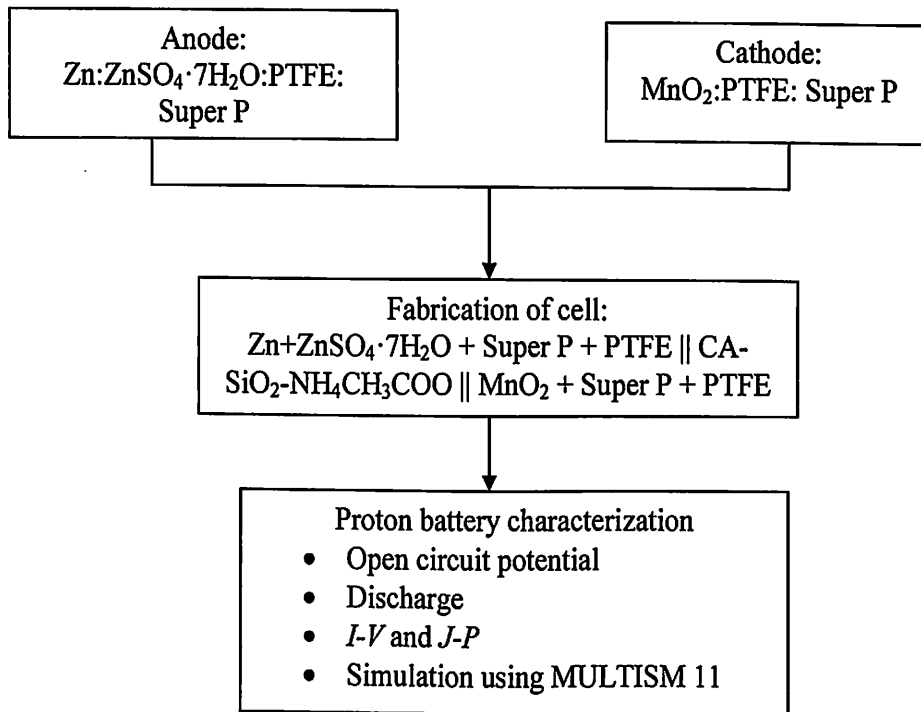


Figure 2.4: Fabrication and characterization test of Zn+ZnSO₄·7H₂O + Super P + PTFE || CA-SiO₂-NH₄CH₃COO || MnO₂ + Super P + PTFE proton battery.

CHAPTER 3

RESULTS AND DISCUSSIONS

3.1 Introduction

In this chapter, the properties of porous chitosan acetate-silica membranes, porous chitosan acetate-silica-ammonium acetate electrolyte and fabrication of the properties of $Zn+ZnSO_4 \cdot 7H_2O$ /porous chitosan acetate-silica-ammonium acetate membranes/ MnO_2 proton battery coin cell. The discussion of current results will be related to the theoretical equation as mentioned earlier in Chapter 2. This chapter will be divided into three sections.

- a) The first section will focus on the results of the porous chitosan acetate-silica membranes:
 - i) Field emission scanning electron microscopy analysis (FESEM), energy dispersive X-ray spectroscopy (EDX) and average of pore sizes.
 - ii) X-ray diffraction analysis (XRD) and crystallite size
 - iii) Fourier transform infrared analysis (FTIR)
 - iv) Thermogravimetric analysis (TGA) and Differential scanning calorimetry (DSC)

b) The second section will highlight the porous chitosan acetate-silica-ammonium acetate electrolyte electrochemical results including:

- i) Nyquist and conductivity plot at room and elevated temperature
- ii) Temperature dependence and activation energy (E_a) plot
- iii) Linear sweep voltammetry (LSV) and cyclic voltammetry (CV)

b) The third section will highlight the properties of Zn+ZnSO₄·7H₂O/porous chitosan acetate-silica-ammonium acetate membranes/MnO₂ proton battery coin cell including:

- i) Open circuit potential (OCP) of proton battery
- ii) Discharge profile of proton battery
- iii) Current voltage ($I-V$) and current density-power density ($J-P$) curves
- iv) Simulation of proton battery via MULTISIM 11 compared with the actual performance of the fabricated batteries.

3.2 Porous CA-SiO₂ Membranes Properties

3.2.1 Morphology and Pore Sizes Analysis

The micrographs of chitosan powder, chitosan acetate (CA) and porous CA-SiO₂ membranes are shown in Figure 3.1. Normally, chitosan powder with bulky surface is shown in Figure 3.1a. The cross section of CA membrane was clear and dense (Figure 3.1b). Figure 3.1c depicted the dense and jagged fleck cross section of CA4S before immersed in NaOH. Meanwhile, the cross section of CA-SiO₂ membranes turned into porous membranes with different pores shape after SiO₂ was dissolved in different concentrations of NaOH (Figure 3.1d-g). The pores of membranes were crumple at first (CA4S1.3N) and growth little by little (CA4S3.0N, CA4S5.0N and CA4S8.0N).

The pores shapes of porous SiO₂-CA membranes were highly dependent on the concentration of NaOH.

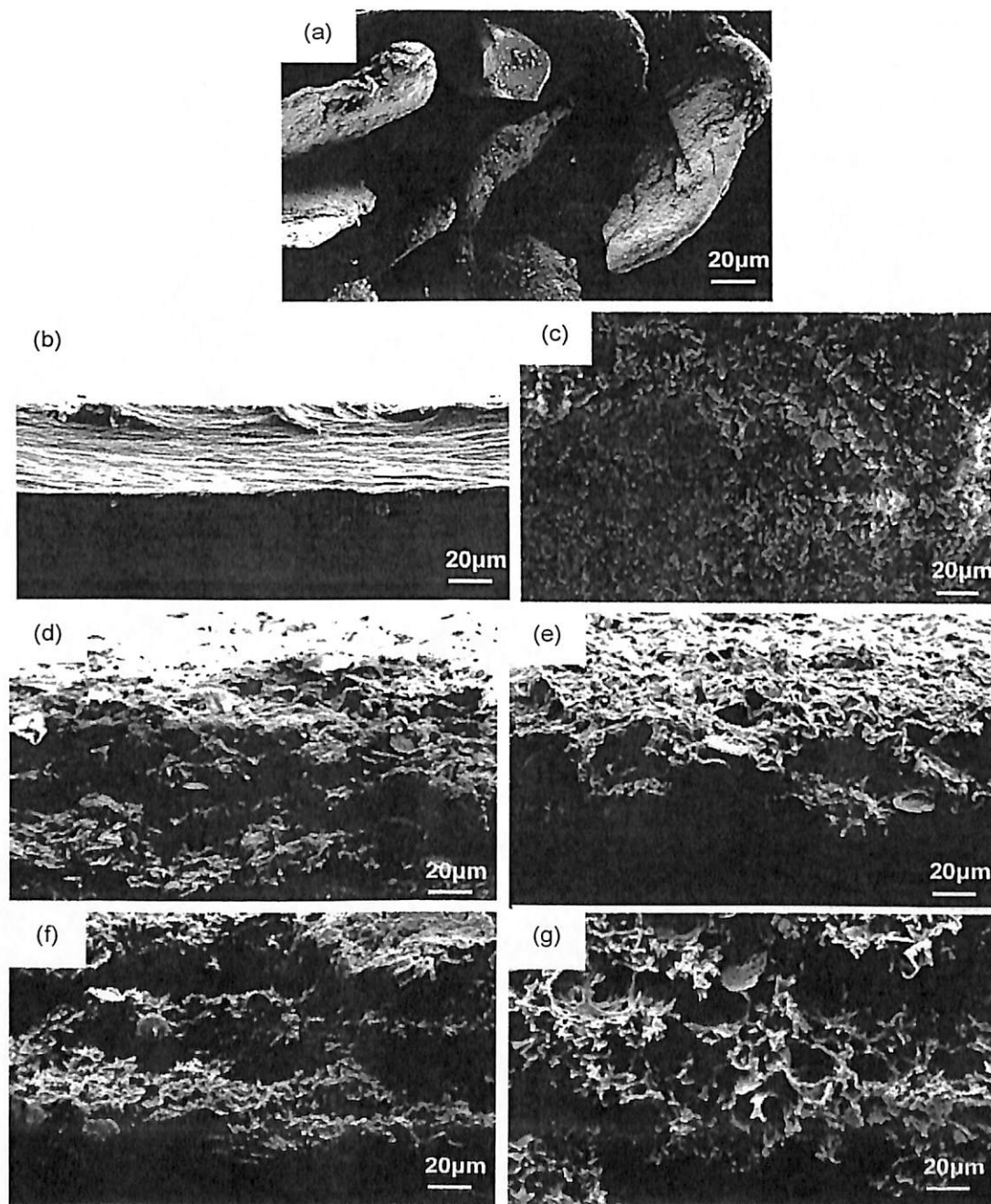
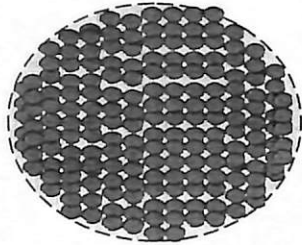
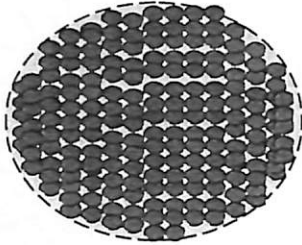
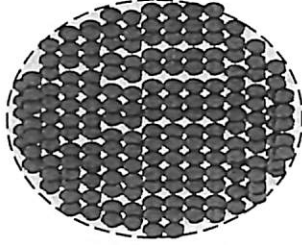
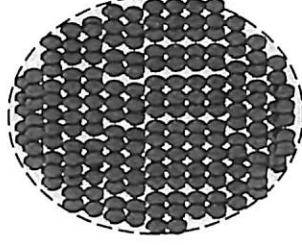
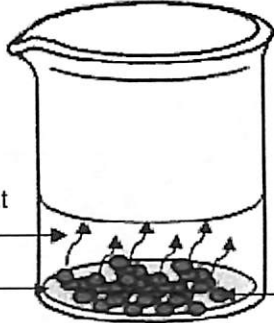
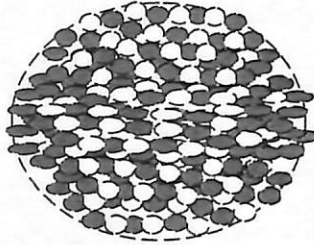
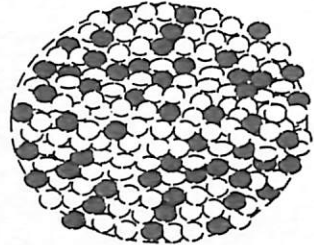
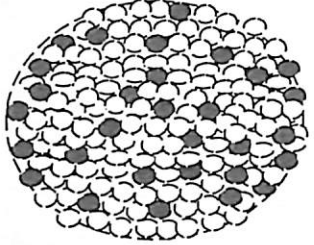
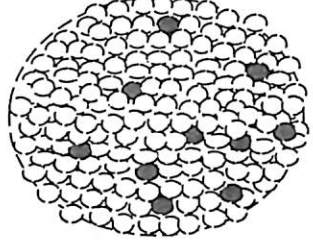


Figure 3.1: Surface morphology of (a) chitosan powder, (b) cross section image of chitosan acetate membrane, porous chitosan-SiO₂ membrane with ratio 1:4 after (c) before and after immerse in (d) 1.3, (e) 3.0, (f) 5.0 and (g) 8.0 M NaOH.

Further discussion on removal SiO_2 particles from membrane process is illustrated in Table 3.1. The pore shapes of CA4S1.3N, CA4S3.0N and CA4S5.0N membranes were not uniform and agglomeration still occurred after immersed in low concentration of NaOH. Herein, SiO_2 was not fully dissolved and still trapped inside membrane (grey colour of particles). The SiO_2 particles attempted to dissolve in NaOH. When NaOH concentration was up to 8.0 M, the SiO_2 dissolved well in NaOH. This is because a sufficient concentration of NaOH can pull out SiO_2 from membranes and dissolved in NaOH. Hence, the porous membranes with uniform pore shape were produced.

The element analysis by EDX represents in Figure 3.2, it showed the different composition of chitosan powder, CA membrane and porous SiO_2 -CA membranes (tables inside). The composition of Si decreased when increasing concentrations of NaOH same circumstances as clarified in Table 3.2.

Table 3.1: Illustration of removal SiO_2 from porous SiO_2 -chitosan membrane.

Samples	CA4S1.3N	CA4S3.0N	CA4S5.0N	CA4S8.0N
Before immerse in NaOH				
During immerse in NaOH	<p>SiO_2 particles dissolved in different NaOH concentration (1.3, 3.0, 5.0 and 8.0 M)</p>  <p>NaOH solution at different concentrations</p> <p>SiO₂-chitosan membrane</p> <p>SiO₂ particles</p>			
After immerse in NaOH				
	<p>● SiO_2 particles before chitosan membrane immerse in NaOH</p> <p>○ Pores after SiO_2 particles dissolve in NaOH from chitosan membrane</p>			

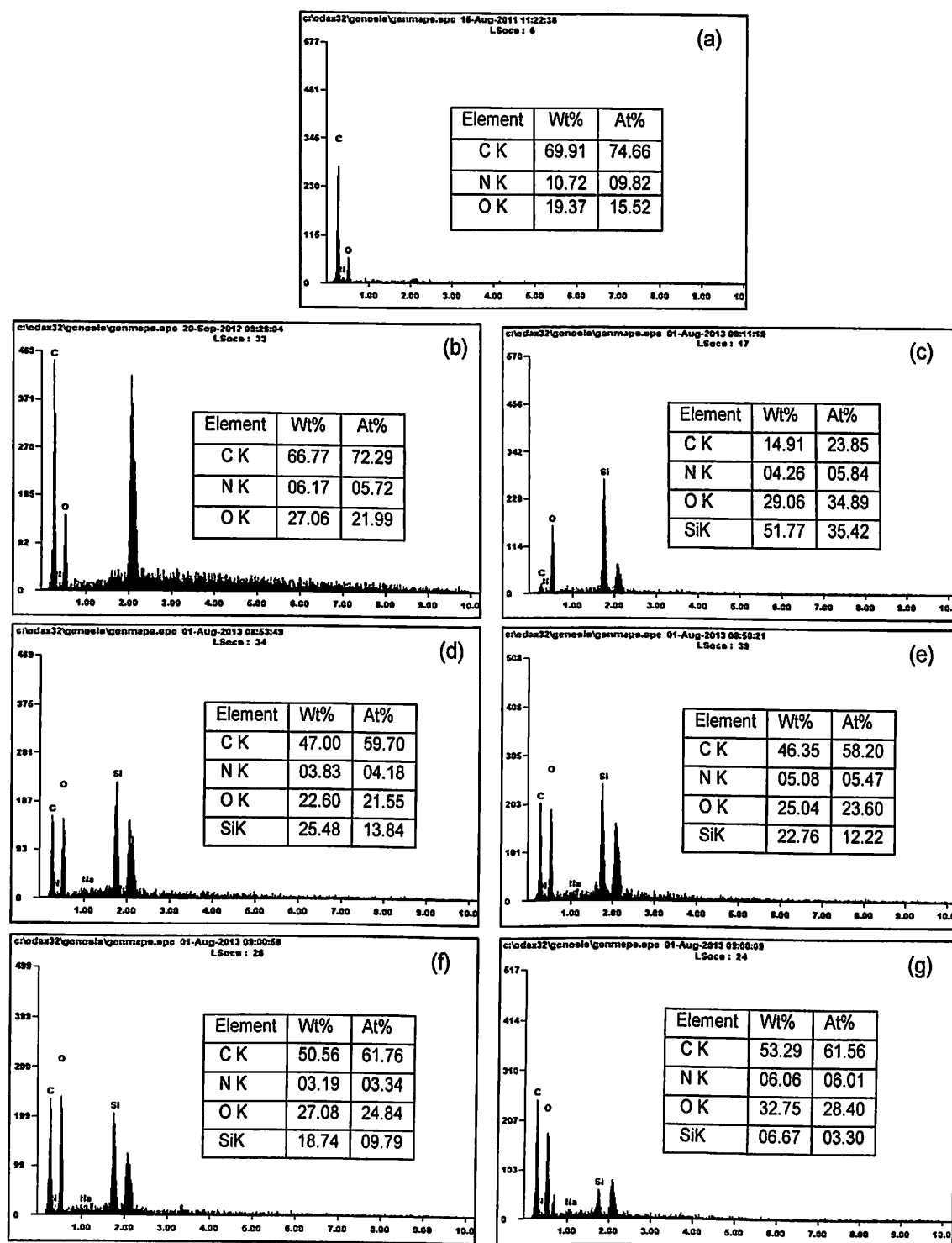


Figure 3.2: EDX of (a) chitosan powder, (b) chitosan acetate membrane (c) CA4S, (d) CA4S1.3N, (e) CA4S3.0N, (f) CA4S5.0N and (g) CA4S8.0N.

Table 3.2: Composition of all membranes after immersed in 1.3, 3.0, 5.0 and 8.0 M NaOH.

Sample	Si		O	
	(Wt %)	(At %)	(Wt %)	(At %)
CA4S	51.77	35.42	29.06	34.89
CA4S 1.3N	25.48	13.84	22.60	21.55
CA4S 3.0N	22.76	12.22	25.04	23.60
CA4S 5.0N	18.74	09.79	27.08	24.84
CA4S 8.0N	06.67	03.30	32.75	28.40

Figure 3.3 shows the average pore size of porous CA-SiO₂ membranes calculated from FESEM results. The pores started to form when membranes were immersed in NaOH. The pore sizes for all membranes were increased gradually especially for CA4S1.3N, CA4S3.0N and CA4S5.0N. However, as mention earlier (Figure 3.1 and Table 3.1) the formation of pore accordingly with SiO₂ shape, which is not uniform and agglomerate. Generally, agglomeration of these particles is caused by the high surface energy of ceramics. This is a common problem that weaken the efficiency of the ceramic filler (Liu et al., 2003). Therefore, this would affect the average pore size of porous CA-SiO₂ membranes. For these samples, the low concentrations of NaOH solution lower the ability of SiO₂ to dissolve in NaOH. Most of SiO₂ in deep membrane cannot be reached by NaOH solution. Thus, the pores size much smaller in a range between 4.7 to 5.0 μm .

Nevertheless, after immersed CA4S8.0N membrane in 8.0 M NaOH, porous membranes with largest average pore sizes (5.9 μm) and uniform pore shape were produced. The higher concentration of NaOH may dissolve large amount of SiO₂ particles in NaOH. Only a small amount of SiO₂ still trapped in deep membrane and not significantly affected the porous structure of membrane. The results are almost similar with previous studies on removal SiO₂ particles from chitosan membrane using NaOH as porogen removal solution based on morphology, removal SiO₂

3.2.2 Structural and Degree of Crystallinity Analysis

The XRD pattern of chitosan powder, CA, SiO₂, CA4S, CA4S1.3N, CA4S3.0N, CA4S5.0N and CA4S8.0N membranes are shown in Figure 3.4. The broad peak at $2\theta = 20^\circ$ is the signature of pure chitosan powder. However, the peak vanished after chitosan powder dissolve in acetic acid. Meanwhile, there is a small peak at $2\theta = 22^\circ$ for SiO₂. When SiO₂ were dispersed in CA solution, the peak at $2\theta = 20$ and 22° become broad. After CA-SiO₂ membranes immersed in NaOH, the intensity of $2\theta = 22^\circ$ continue to increase slowly. Only broad peak at $2\theta = 20^\circ$ can be seen for CA4S8.0N.

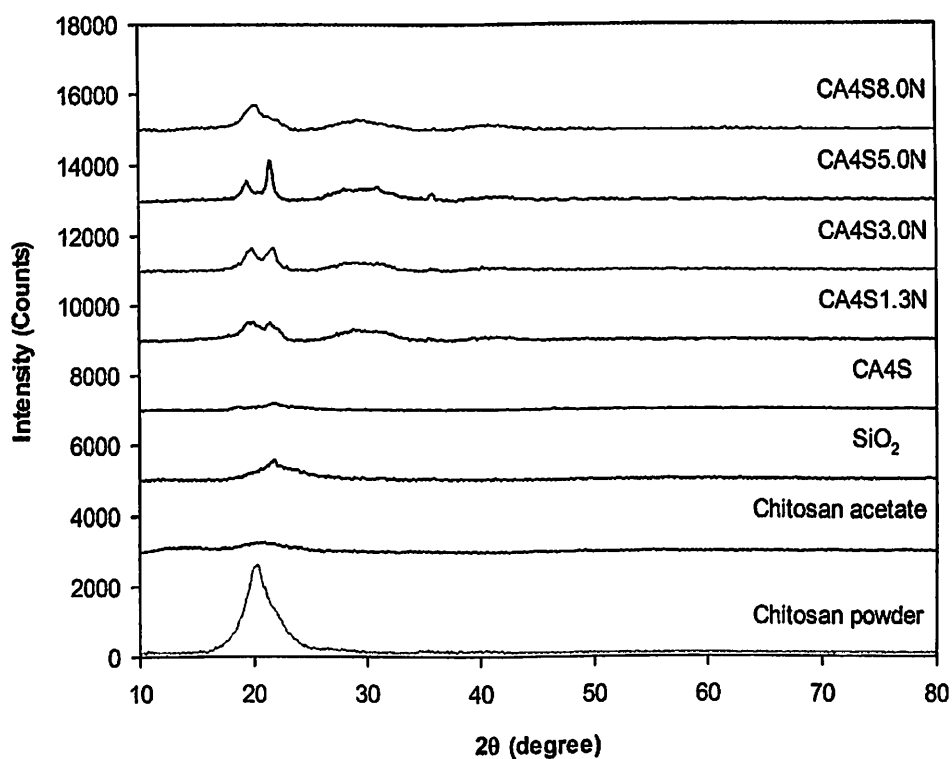


Figure 3.4: XRD of chitosan powder, chitosan acetate membrane, SiO₂, CA4S, CA4S1.3N, CA4S3.0N, CA4S5.0N and CA4S8.0N.

The deconvolution of XRD for chitosan powder, CA membrane, SiO₂, CA4S, CA4S1.3N, CA4S3.0N, CA4S5.0N and CA4S8.0N (Figure 3.5) provides the details changing of membranes crystalline structure showed in Figure 3.4. The highly crystalline of chitosan powder turn into amorphous structure after dissolve in acetic acid for CA membrane (Figure 3.5a and b). This can be seen by the decreasing intensity peak at $2\theta = 20^\circ$ and broad peak at $2\theta = 15^\circ$ of CA membrane. Figure 3.5c shows the SiO₂ is highly crystalline based on the high intensity peak at $2\theta = 22^\circ$ similar with previous study on structural analysis of SiO₂ (Bu et al., 2014). When SiO₂-CA membranes immersed in NaOH, the intensity of $2\theta = 22^\circ$ were slightly increase, but not too notable since the whole XRD peaks for CA4S1.3N, CA4S3.0N and CA4S5.0N still broad (Figure 3.5d-f). In addition, the intensity of humps at $2\theta = 20, 30$ and 40° for these three samples maintain at same range and broad. This endorses the fact that these membranes still had amorphous structure. However, Figure 3.5e shows only broad peak at $2\theta = 20, 30$ and 40° appeared for CA4S8.0N. The shifting of all peaks demonstrated that structure of membrane has been changed.

After immersed in 8.0 M NaOH, the crystallinity of membrane decreased, increased its amorphous structure compared with membranes immersed in lower concentration of NaOH (1.3, 3.0 and 5.0 M). Normally, the formation of amorphous polymer phases at the surface can be brought by the ceramic filler (Liu et al., 2003). In this study, the sufficient concentration of NaOH will attract more SiO₂ particles to dissolve into NaOH solution. Hence, produce amorphous membrane. Insufficient concentration of NaOH will cause insolubility of SiO₂. Thus, the membranes were not fully amorphous since some parts contained high crystalline of SiO₂ ceramic filler.

The degrees of crystallinity for chitosan powder, CA and porous SiO₂-CA membranes are further determined from XRD analysis as seen in Figure 3.6. The chitosan powder had the highest crystallinity. Meanwhile, the crystallinity for CA decreased to 44 %. Furthermore, the crystallinity of porous SiO₂-CA membranes increased rapidly after mixed SiO₂. The crystallinity increased gradually after immersed in different concentration of NaOH. However, the crystallinity decreased when porous SiO₂-CA membrane was immersed in 8.0 M NaOH. Table 3.3 listed the degree of crystallinity all membranes after immersed in 1.3, 3.0, 5.0 and 8.0 M NaOH.

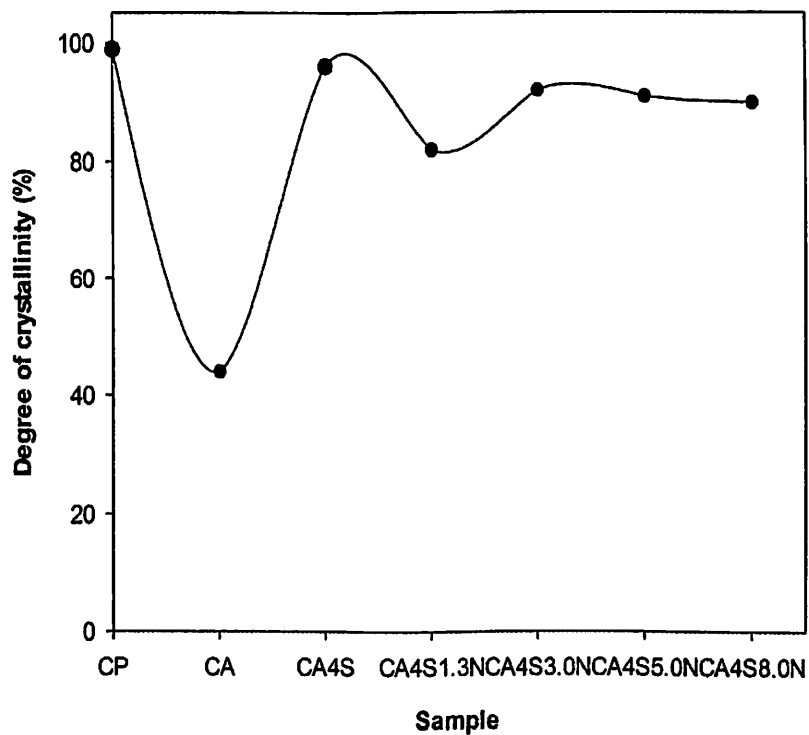


Figure 3.6: Degree crystallinity of chitosan powder, chitosan acetate membrane, SiO₂, CA4S, CA4S1.3N, CA4S3.0N, CA4S5.0N and CA4S8.0N.

Table 3.3: Degree of crystallinity all membranes after immersed in 1.3, 3.0, 5.0 and 8.0 M NaOH.

Sample	Degree of crystallinity (%)
Chitosan powder (CP)	99
Chitosan acetate (CA)	44
CA4S	96
CA4S 1.3N	82
CA4S 3.0N	92
CA4S 5.0N	91
CA4S 8.0N	90

The decreasing crystallinity of CA membrane is due to the changing of high crystalline chitosan powder to amorphous structure after dissolve in CH_3COOH . Normally, polymers are not 100 % crystalline since too difficult for polymers to align the chains. Therefore, the dominant amorphous structure of CA membrane decreased the crystallinity. When high crystalline of SiO_2 was mixed to the CA membrane, the crystallinity of membranes increased. This attributed by the shifting of membrane molecular chains after immersed in 1.3, 3.0 and 5.0 M of NaOH. The poor condition for SiO_2 to dissolve affected the structure of membranes. Nevertheless, the cystallinity of porous SiO_2 -CA membrane slightly decreased after immersed in 8.0 M NaOH. This proved that at the sufficient concentration of porogen removal solution, the SiO_2 will dissolve in NaOH (Zeng and Ruckenstein, 1996; Santos et al., 2008). Thus, the crystallinity of membranes decreased.

3.2.3 Chemical Interaction Analysis

The FTIR analysis and chemical interaction of chitosan powder, CA, porous CA4S1.3N, CA4S3.0N, CA4S5.0N, CA4S8.0N membranes and SiO₂ are illustrated in Figure 3.7. The broad peak at 3550-3050 cm⁻¹ in Region 1 could be assigned to the axial stretching vibration of O–H superposed to the N–H stretching band and chitosan inter-hydrogen bonds (Enescu et al., 2009).

The small peak at 2990-2830 cm⁻¹ in Region 2 is denoted as two bands for CH₂ group for all samples except CA4S membrane and SiO₂. This is attributed by the high amount of SiO₂ in CA4S membrane before immersed in NaOH. Meanwhile, the peak of 1650-1550 cm⁻¹ in Region 3 refer to the symmetry of C=O stretch peak (Tran et al., 2013). Herein, the cation of CH₃COOH solution interacted with the nitrogen atom of NH₂ in chitosan. Consequently, NH₂ and other bands shifted for CA membrane. However, this peak became smaller proportional with NaOH concentration used to immerse porous membranes. This is due to the effect of inclusion and removal of SiO₂ in CA2.0S30N membrane.

In Region 4, a few peaks exhibits in a range 1450-1250 cm⁻¹ presented the existence of C–O stretch or OH deformation and C–C(O)–C stretch (acetates). The O–H band at 1400 cm⁻¹ is referred to CA after dissolve in CH₃COOH solution. Moreover, the C–O stretch at 1269 cm⁻¹ is also denoted to CA after dissolve in CH₃COOH solution. Both of these peaks disappeared in all membranes after porogen removal of SiO₂ occurred in NaOH solutions.

Another small peak in a range of 1200-1150 cm⁻¹ is shown in Region 5 could be assigned to C–N stretch of chitosan powder CA, and all porous membranes. In Region 6, there are several functional group appeared in a range 1080-920 cm⁻¹ which are C–O–H deformation, C–NH₂ and C–OH deformation of chitosan powder

CA and Si-O-Si, Si-O-C of porous CA4S1.3N, CA4S3.0N, CA4S5.0N, CA4S8.0N membranes and SiO₂ (Pattnaik et al., 2011; Ramesh and Liew, 2012).

The peak of 895-620 cm⁻¹ presented in Region 7 could be assigned to the Si-O-Si, Si-CH₃, N-H bend and O-C=O of chitosan powder, CA, SiO₂ and porous CA4S1.3N, CA4S3.0N, CA4S5.0N, CA4S8.0N membranes (Pattnaik et al., 2011; Ramesh and Liew, 2012). The shifting of peak for Si-O-Si, Si-O-C for all porous membranes proved that after immersed in NaOH, the SiO₂ particles removed from membrane. As a result, the intensity of these peaks also decreased.

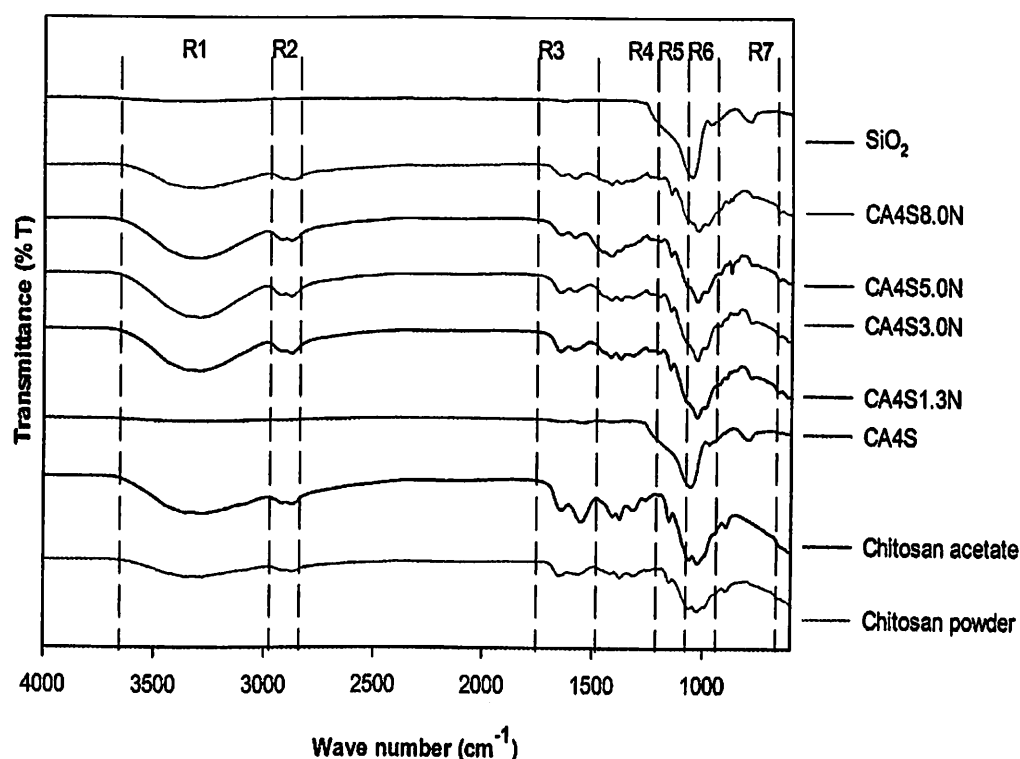


Figure 3.7: FTIR of chitosan powder, chitosan acetate, CA4S1.3N, CA4S3.0N, CA4S5.0N, CA4S8.0N membranes and SiO₂.

All the chemical interaction between chitosan powder, acetic acid and SiO₂ occurred in this study is illustrated in Figure 3.8. After immersed in NaOH, the functional group of porous CA2.0S30N membrane shifted. This showed that SiO₂

particles were removed easily from membrane at optimum concentration of NaOH porogen removal solution (Zeng and Ruckenstein, 1996; Clasen et al., 2006; Santos et al., 2008; Mei et al., 2012). The functional group of all membranes are listed in Table 3.7.

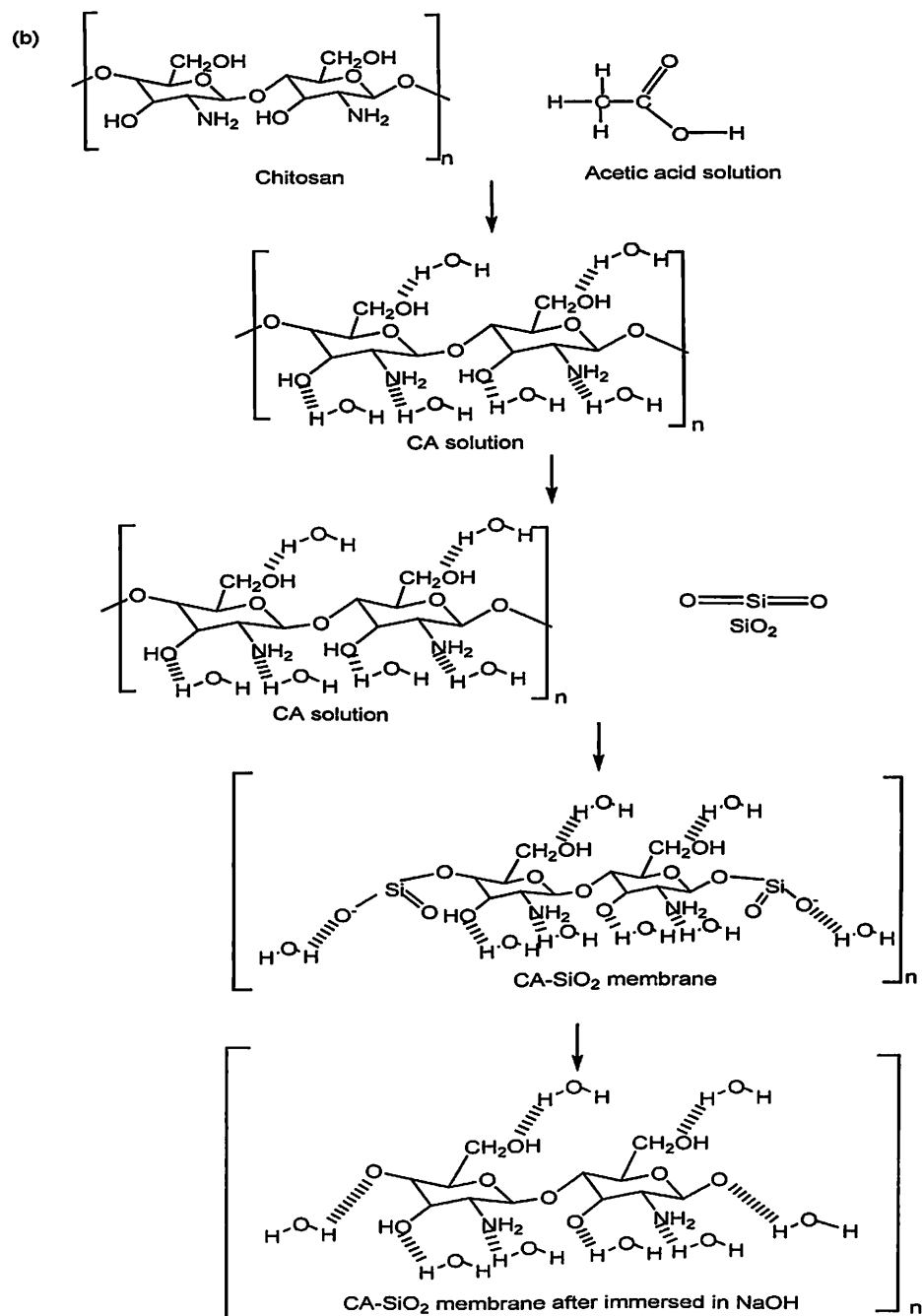


Figure 3.8: Chemical interaction between chitosan powder, acetic acid and SiO₂.

Table 3.4: Functional group of all membranes.

Region	Wavenumber (cm ⁻¹)	Functional group
R 1	3550-3050	Stretching vibration of N-H and O-H
R 2	2990-2830	Two bands for CH ₂ group
R 3	1650-1550	C=O stretch N-H bend
R 4	1450-1250	C-O stretch / OH deformation C-C(O)-C stretch (acetates)
R 5	1200-1150	C-N stretch
R 6	1080-920	C-O-H deformation Si-O-Si Si-O-C C-NH ₂ C-OH deformation
R7	895-620	Si-CH ₃ N-H bend R-NH ₂ O-C=O

3.2.4 Porous CA-SiO₂ Membrane: Thermal analysis

The percentage of chitosan powder, chitosan acetate, CA4S1.3N, CA4S3.0N, CA4S5.0N and CA4S8.0N membranes weight loss was determined from thermogravimetric analysis (TGA). The first phase is desorption process followed by total decomposition. The desorption process for all samples were occurred in a range 100-120°C, with a steady weight loss about 10-15 %. This water desorption process range of temperature and percentage of weight loss is in agreement with previous study on chitosan film thermal properties (Matet et al., 2013). The total decomposition began in the region between 200-300°C with rapid weight loss in a range between 20-60 % . This percentage of weight loss increase after immersed in NaOH porogen removal solution.

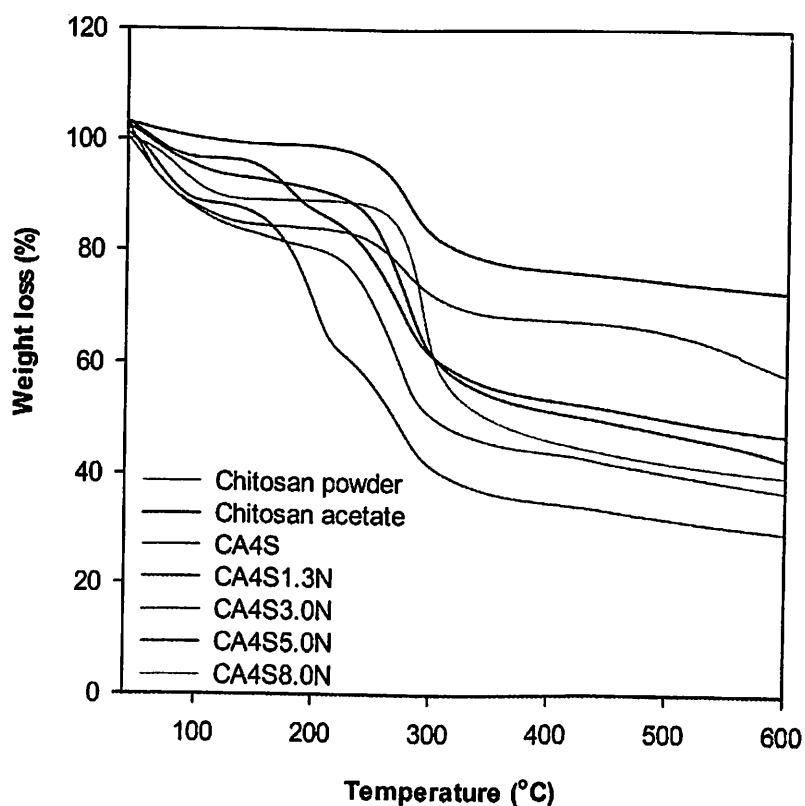


Figure 3.9: TGA thermograms of chitosan powder, chitosan acetate, CA4S1.3N, CA4S3.0N, CA4S5.0N and CA4S8.0N membranes.

The differential scanning calorimetry (DSC) shows the chitosan powder, chitosan acetate, CA4S1.3N, CA4S3.0N, CA4S5.0N and CA4S8.0N membranes are shown in Figure 3.10. The noticeable endothermic peak emerged in a range between 120-130°C, which represents the melting of chitosan membrane crystallinity. The melting peak of CA4S membrane much higher since this membrane was not immersed in NaOH and still contain higher amount of SiO₂. However, this peak started to decrease after immersed in NaOH. The melting point range obtained in this study is almost similar with previous study on poly(lactic acid)/starch/chitosan blended matrix (Bie et al., 2013).

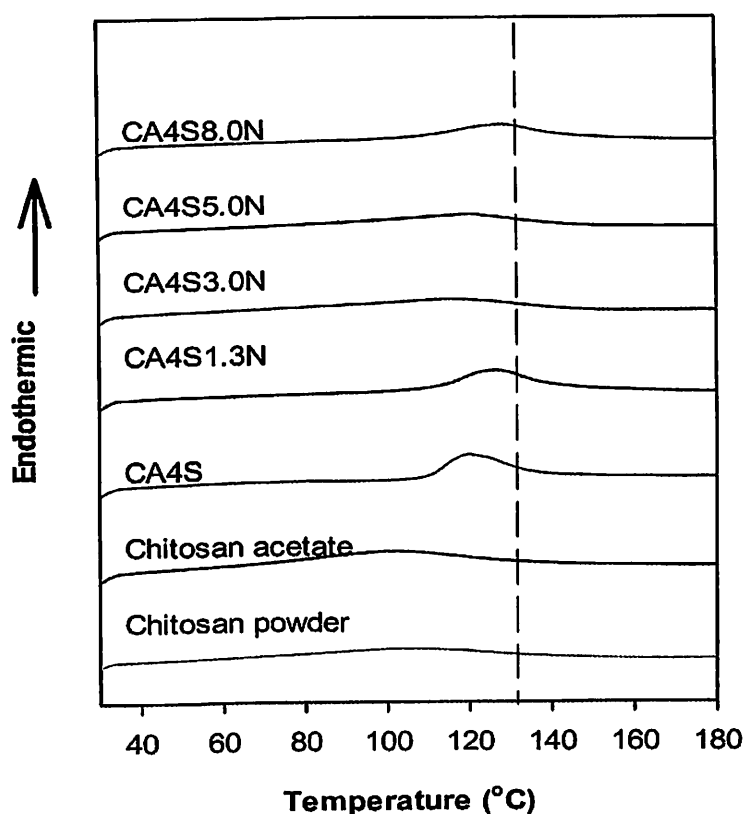


Figure 3.10: DSC of chitosan powder, chitosan acetate, CA4S1.3N, CA4S3.0N, CA4S5.0N and CA4S8.0N membranes.

was obtained in 5.0AA. No existing capacitance component can be seen. However, the R_b increased for 7.0AA due to the high resistance in $\text{NH}_4\text{CH}_3\text{COO}$ solution. All the samples show only resistive component which is attributed to the addition concentrations of $\text{NH}_4\text{CH}_3\text{COO}$ into the system. The bulk resistance values of $\text{NH}_4\text{CH}_3\text{COO}$ were listed in Table 3.5.

Table 3.5: The bulk resistance values of $\text{NH}_4\text{CH}_3\text{COO}$ at different concentrations.

Sample name	Concentration of $\text{NH}_4\text{CH}_3\text{COO}$ (M)	Weight of $\text{NH}_4\text{CH}_3\text{COO}$ (g)	Amount of deionized water (ml)	Bulk resistance, R_b (Ω)
Deionized water	-	-	20	6530.0
1.0AA	1.0	1.54	20	5.5
3.0AA	3.0	4.62	20	3.9
5.0AA	5.0	7.71	20	2.7
7.0AA	7.0	10.79	20	3.0

Figure 3.12 shows the conductivity of $\text{NH}_4\text{CH}_3\text{COO}$ at different concentrations. The conductivity was calculated based on the R_b values Equation 2.1. The conductivity increased inversely proportional with R_b values. The highest conductivity of $(7.0 \pm 0.2) \times 10^{-2} \text{ S cm}^{-1}$ was obtained with 5.0 M of $\text{NH}_4\text{CH}_3\text{COO}$ electrolyte solution. However, the conductivity decreased at 7.0 M $\text{NH}_4\text{CH}_3\text{COO}$ electrolyte solution. At high concentrations of $\text{NH}_4\text{CH}_3\text{COO}$, reassociation (ion pairing) of H^+ took place, which decreased conductivity. The conductivity of $\text{NH}_4\text{CH}_3\text{COO}$ at different concentrations is tabulated in Table 3.6.

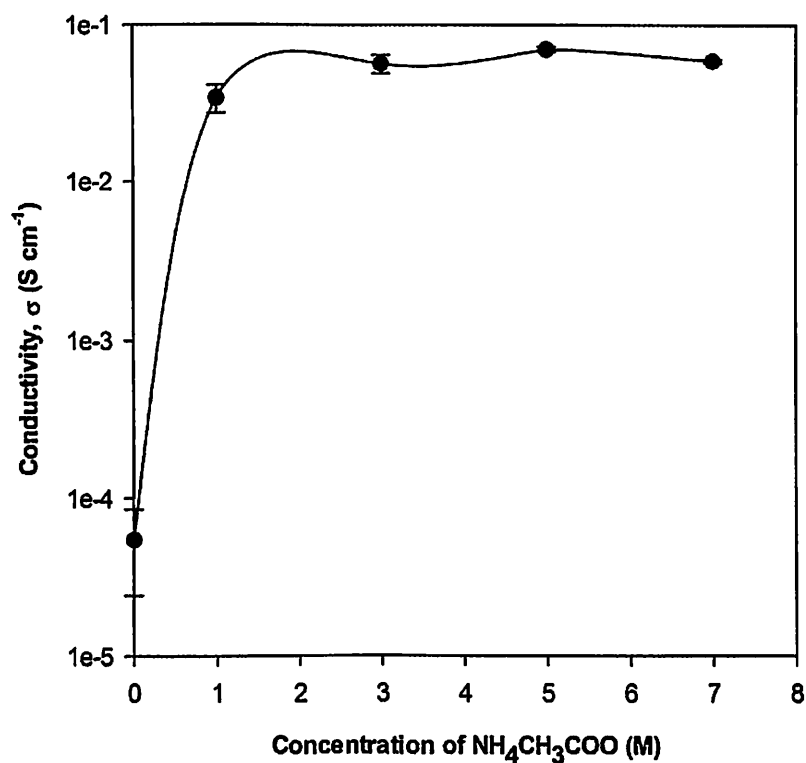


Figure 3.12: Conductivity of $\text{NH}_4\text{CH}_3\text{COO}$ at different concentrations.

Table 3.6: The conductivity of $\text{NH}_4\text{CH}_3\text{COO}$ at different concentrations.

Sample name	Concentration of $\text{NH}_4\text{CH}_3\text{COO}$ (M)	Weight of $\text{NH}_4\text{CH}_3\text{COO}$ (g)	Amount of deionized water (ml)	Bulk resistance, R_b (Ω)
Deionized water	-	-	20	6530.0
1.0AA	1.0	1.54	20	5.5
3.0AA	3.0	4.62	20	3.9
5.0AA	5.0	7.71	20	2.7
7.0AA	7.0	10.79	20	3.0

Since CA4S8.0N membrane shows good morphology, structural, thermal and chemical properties, this membrane has been chosen to immerse in 5.0 M $\text{NH}_4\text{CH}_3\text{COO}$ electrolyte solution. The Nyquist plot of CA4S8.0N and CA4S8.0N after immersed in $\text{NH}_4\text{CH}_3\text{COO}$ electrolyte solution for 2 days (designated as

The temperature dependence for CA4S8.0N and CA4S8.0N5AA-2D were performed within a range of 25 to 90°C as represented in Figure 3.14. The dependencies for both samples can be fitted reasonably by linear lines in this temperature range with correlation coefficients (R^2) of ~ 0.9 . The conductivity of samples increased proportionally with the temperature and showed Arrhenius type relation. Similar to previous conductivity values at room temperature, the conductivity also increased for CA4S8.0N5AA-2D after immersed in $\text{NH}_4\text{CH}_3\text{COO}$ electrolyte solution for 2 days.

The free volume model can be described the behavior of conductivity enhancement with temperature (Rajendran and Uma, 2000). This free volume can expand easily proportional with increasing temperature for CA4S8.0N5AA-2D compared with CA4S8.0N. When the temperature increased, the overall mobility of H^+ ions, solvated molecules and potato starch segments can move into the expansion of free volume. This conducts in increasing of H^+ ions mobility and segmental mobility that will assist H^+ ion transport and almost balance for the hindering effect of H^+ ion clouds. In contrast, there is no existence H^+ ion in CA4S8.0N. Even the free volume expanded at high temperature, but the free volume could not contribute to increase conductivity.

The activation energy for CA4S8.0N and CA4S8.0N5AA-2D were calculated based on Equation 2.2-2.8. The activation energy for CA4S8.0N and CA4S8.0N5AA-2D were 0.2 and 0.03 eV, respectively. The sufficient amount of H^+ ions is utterly assisted to lower activation energy. The energy needed for H^+ ions to hop together on the coordinating site of CA4S8.0N5AA-2D was lower compared with CA4S8.0N (membrane without H^+ ion).

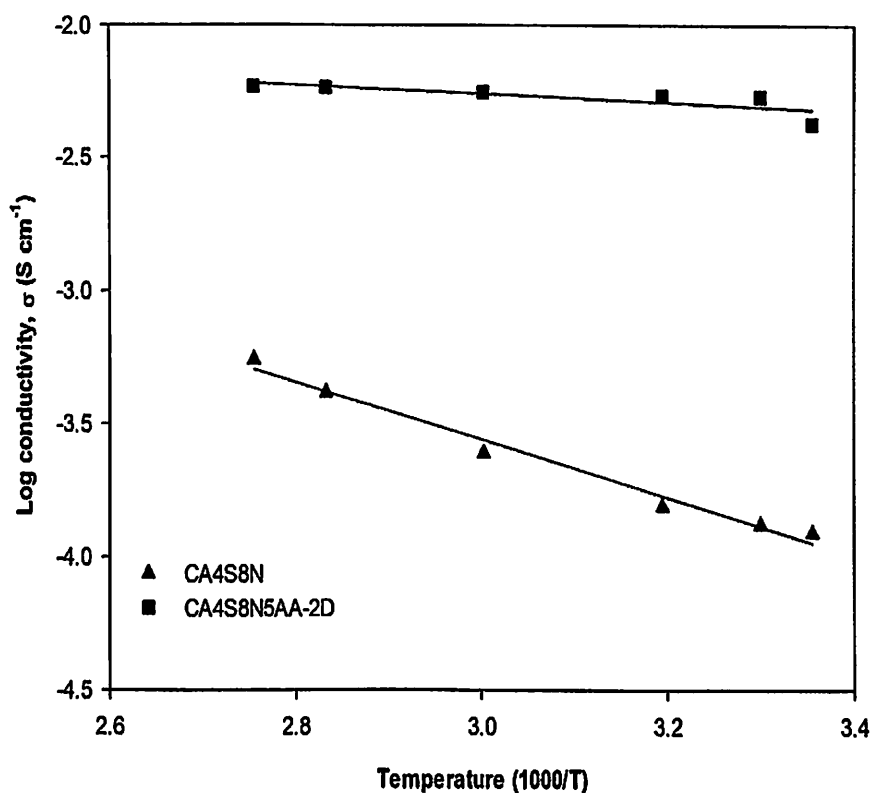


Figure 3.14: The temperature dependence of CA4S8.0N and CA4S8.0N5AA-2D.

3.3.2 Linear Sweep Voltammetry

The linear sweep voltammetry (LSV) of CA4S8.0N and CA4S8.0N5AA-2D are presented in Figure 3.15. The breakdown voltages can be determined by the extrapolating of the straight line from LSV curves. The LSV curve has a breakdown voltage of 1.5 V for CA4S8.0N (Figure 3.15a). Meanwhile the LSV curve has a breakdown voltage of 1.8 V for CA4S8.0N5AA-2D (Figure 3.15b). Generally, the optimal value of breakdown voltage for electrolyte added with other materials such as salts is in between 1.84-1.89 V (Koh et al., 2011). Hence, the LSV value of CA4S8.0N5AA-2D obtained in this study is almost similar with optimal value of breakdown voltage for electrolyte.

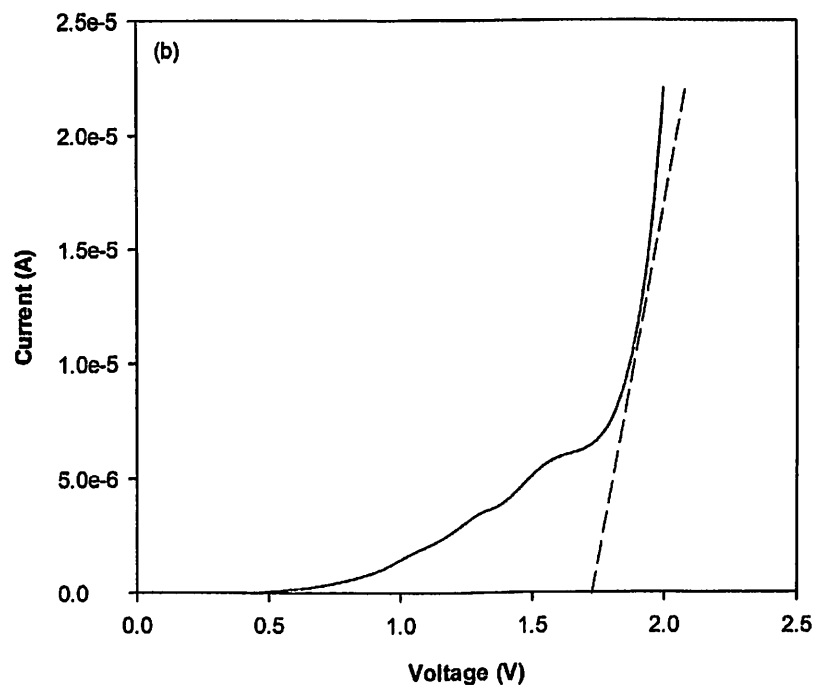
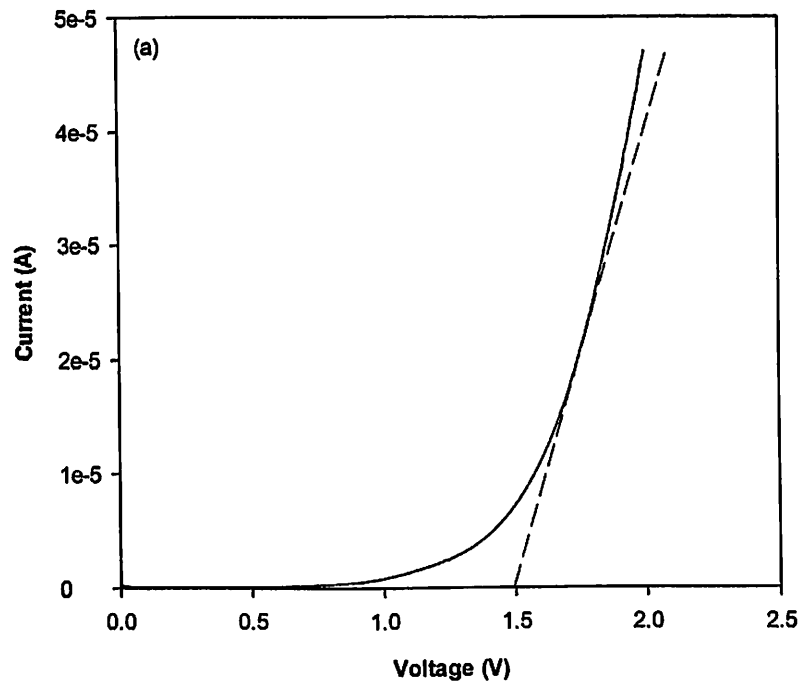


Figure 3.15: Linear sweep voltammetry curves of (a) CA4S8.0N and (b) CA4S8.0N5AA-2D.

3.3.3 Cyclic Voltammetry

The CA4S8.0N5AA-2D was further analyzed using cyclic voltammetry (CV) as shown in Figure 3.16 in order to determine its window stability. The window stability of CA4S8.0N5AA-2D was 3.2 V. When the value of window stability is more than 2.4 V, it can be see that the increasing of currents is due to the increased flow of oxygen gas is evolved. Hydrogen gas is also evolved as the ability to more than -2.8 V. The production of hydrogen and oxygen gas proved that CA4S8.0N5AA-2D membrane suffered to degrade when excess capacity range of 3.2 V at 25°C. In addition, the potential difference of CA4S8.0N5AA-2D (3.2 V) is greater than the stability window of water (1.23 V).

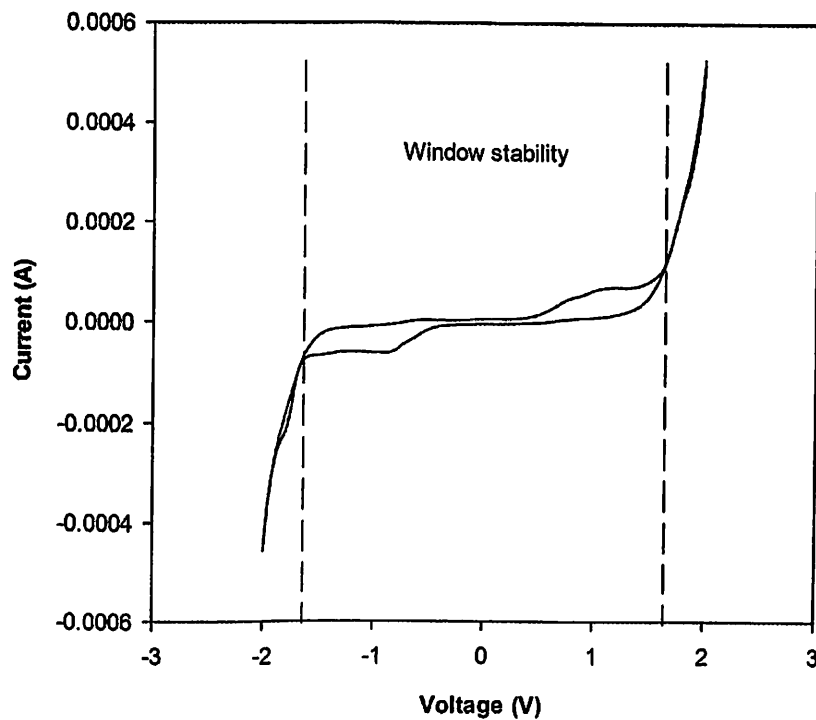


Figure 3.16: Cyclic voltammetry of CA4S8.0N5AA-2D

3.4 Porous CA-SiO₂-NH₄CH₃COO Membrane: Proton Batteries Properties

3.4.1 Discharge Profile

The discharge profile of Zn+ZnSO₄·7H₂O || CA4S8.0N5AA-2D || MnO₂ coin cell at 0.1, 0.2, 0.5 and 1.0 mA are depicted in Figure 3.17. The discharge profile properties are summarized in Table 3.7. The specific discharge capacities increased as the discharge current increased. The specific discharge capacities obtained in this study higher compared with discharge capacities obtained in previous works on proton batteries discharge capacities which were 17.0 mAh (Ng and Mohamad, 2006), 14.7 mAh (Yap and Mohamad, 2007) and 42.7 mAh (Ng and Mohamad, 2008).

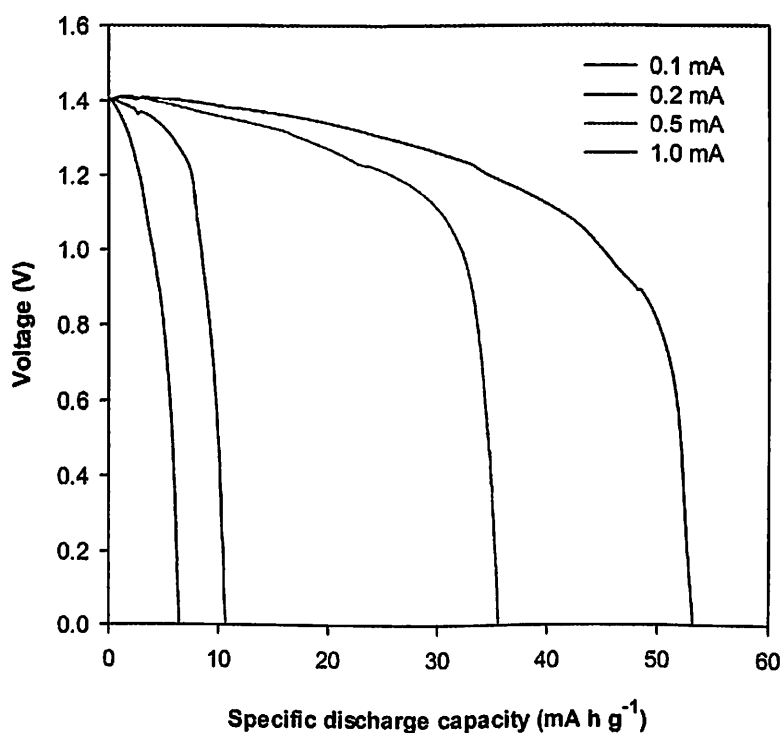


Figure 3.17: The Zn+ZnSO₄·7H₂O || CA4S8.0N5AA-2D || MnO₂ coin cell discharge profile at 0.1, 0.2, 0.5 and 1.0 mA.

Table 3.7: Discharge profile properties at 0.1, 0.2, 0.5 and 1.0 mA.

Discharge current (mA)	Initial voltage (V)	Cutoff voltage (V)	Specific discharge capacity (mAh g ⁻¹)
0.1	1.4	0.0009	6.4
0.2	1.4	0.0083	10.7
0.5	1.4	0.0027	35.6
1.0	1.4	0.0018	53.3

3.4.2 *I-V* and *J-P* Plot

The characteristics of *I-V* and *J-P* of Zn+ZnSO₄·7H₂O || CA4S8.0N5AA-2D || MnO₂ coin cell is shown in Figure 3.18 using current drains ranging from 5.0 μA to 80.0 mA. The voltage dropped from 1.5 V to 0.1 V. The internal resistance (*r*) value was calculated from the gradient of the *I-V* plot, which was 0.02 Ω. The *I-V* curves for both batteries were linear. This result showed that the ohmic contribution was mainly controlled for the polarization of the electrode. The *r* value much lower compared with previous works on proton batteries which were 29.8 Ω (Ng and Mohamad, 2006), 8.5 Ω (Yap and Mohamad, 2007) and 16.8 Ω (Ng and Mohamad, 2008).

The *J-P* curves of Zn+ZnSO₄·7H₂O || CA4S8.0N5AA-2D || MnO₂ coin cell is illustrated in Figure 3.19. Based on the *J-P* curves, the maximum power density was 11.0 mW cm⁻². The maximum power densities attained for both batteries were comparable compared with those in previous studies (Yap and Mohamad, 2007; Ng and Mohamad, 2008).

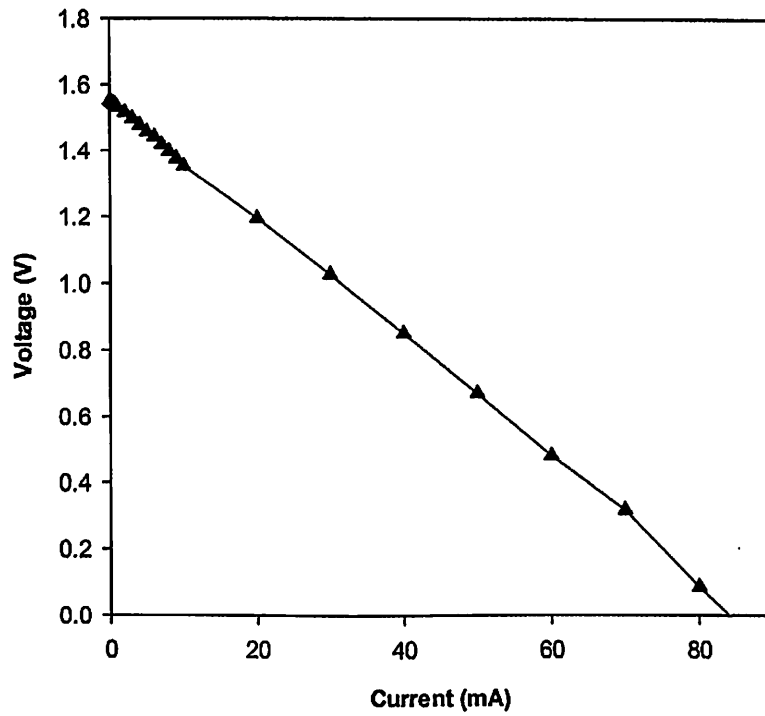


Figure 3.18: Plot of $I-V$ for $\text{Zn}+\text{ZnSO}_4\cdot 7\text{H}_2\text{O} \parallel \text{CA4S8.0N5AA-2D} \parallel \text{MnO}_2$ coin cell.

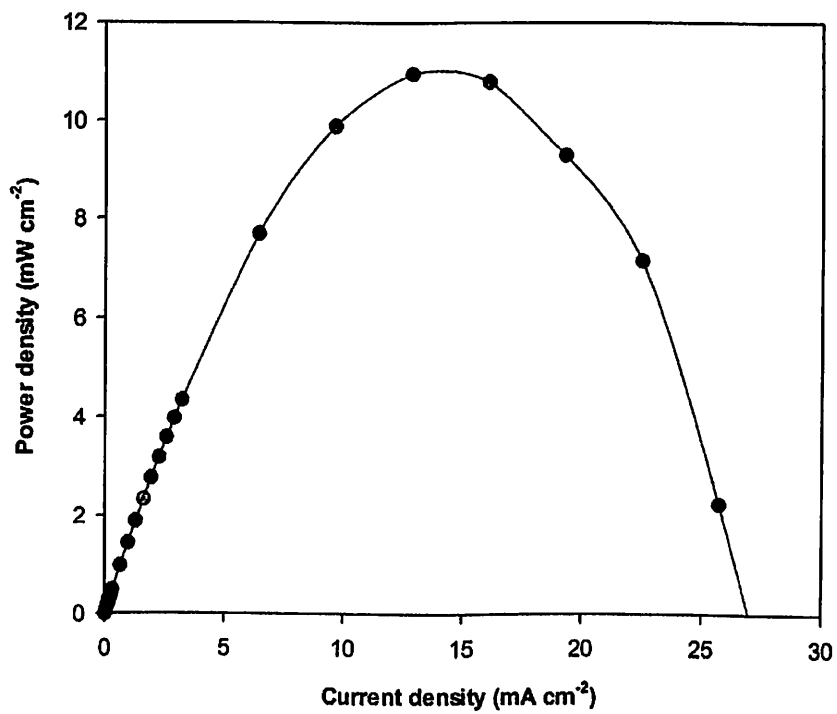
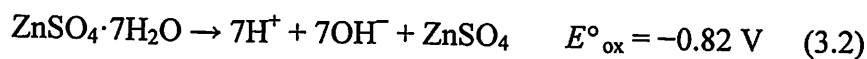


Figure 3.19: Plot of $J-P$ for $\text{Zn}+\text{ZnSO}_4\cdot 7\text{H}_2\text{O} \parallel \text{CA4S8.0N5AA-2D} \parallel \text{MnO}_2$ coin cell.

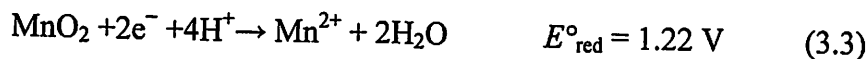
3.4.3 Open Circuit Potential

The OCP of Zn+ZnSO₄·7H₂O || CA4S8.0N5AA-2D || MnO₂ coin cell is presented in Figure 3.20. The OCP of the proton battery was 1.5 V for 8 days. The chemical reaction that probably took place in the proton battery was as follows (Weast, 1977):

At the negative (anode) electrode, Zn was oxidized with the release of two electrons. ZnSO₄·7H₂O provided the source of H⁺ ions as follows:

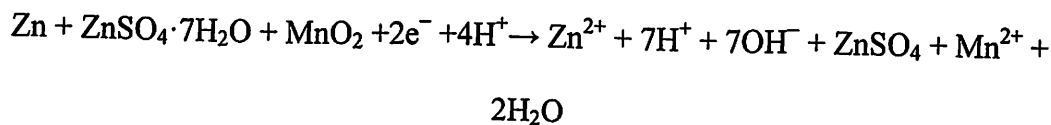


At the positive (cathode) electrode, MnO₂ was reduced with the acceptance of two electrons as follows:



The overall proton battery reaction was calculated based on the standard electrode potential (the oxidation potential is the negative value of the reduction potential) as follows (Linden, 2002):

$$E^{\circ}_{\text{ox}} + E^{\circ}_{\text{red}} = E^{\circ}_{\text{cell}}$$



$$-(0.76 - 0.82) \text{ V} + 1.22 \text{ V} = 1.28 \text{ V} \quad (3.4)$$

The overall reaction should provide the cell with E°_{cell} of 1.28 V. However, the E°_{cells} of both batteries from the current work was 1.5 V. Thus, Equations (3.1) to (3.4) are possible because the fabrication of both batteries achieved higher OCP values than those obtained through theoretical calculation. In the present study, the high conductivity of H⁺ improved the OCP of the coin cells.

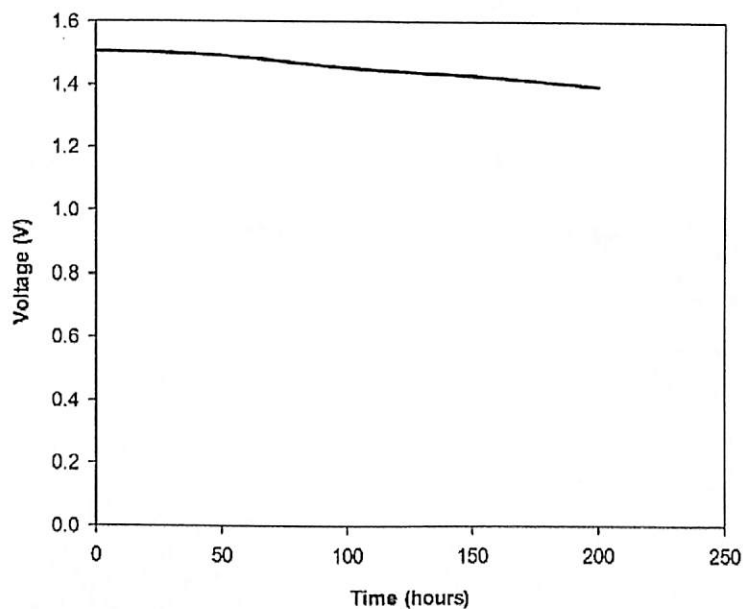


Figure 3.20: The $\text{Zn}+\text{ZnSO}_4 \cdot 7\text{H}_2\text{O} \parallel \text{CA67S8N5A} \parallel \text{MnO}_2$ coin cell open circuit potential.

3.4.4 Application of Proton Batteries

Figure 3.21 shows the virtual and actual combination of two $\text{Zn}+\text{ZnSO}_4 \cdot 7\text{H}_2\text{O} \parallel \text{CA67S8N5A} \parallel \text{MnO}_2$ coin cell to turn on the green light-emitting diode (LED). After 40 hours, the LED was switched off and the voltage dropped from 2.5 to 2.0 V (Figure 3.22).

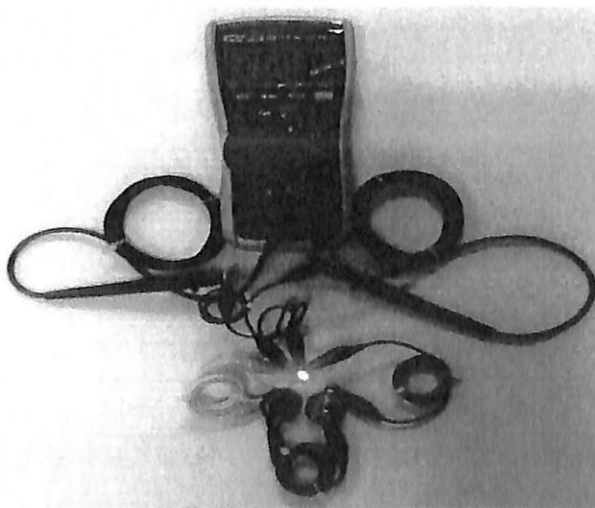


Figure 3.21: The $\text{Zn}+\text{ZnSO}_4 \cdot 7\text{H}_2\text{O} \parallel \text{CA67S8N5A} \parallel \text{MnO}_2$ coin cells actual application with green LED.

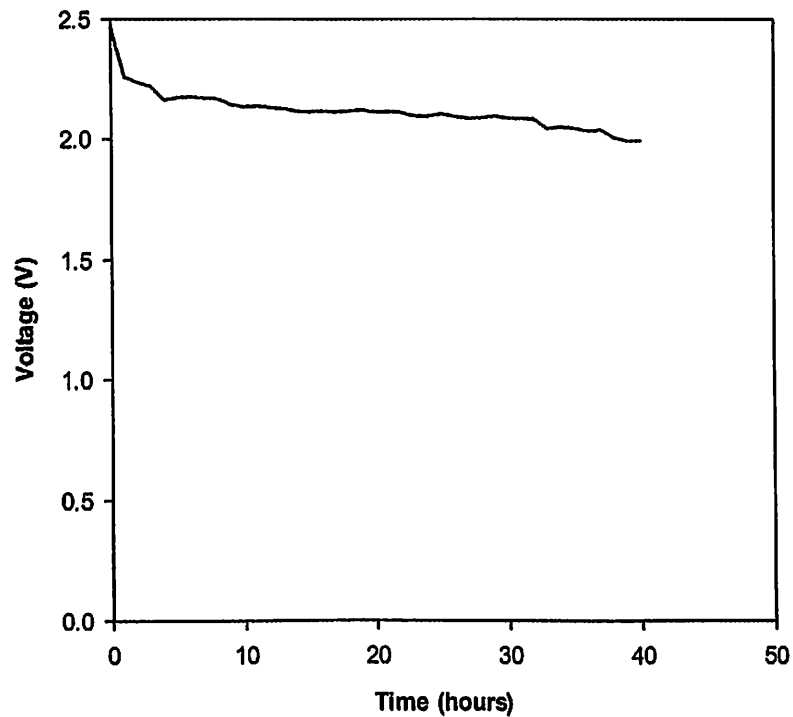
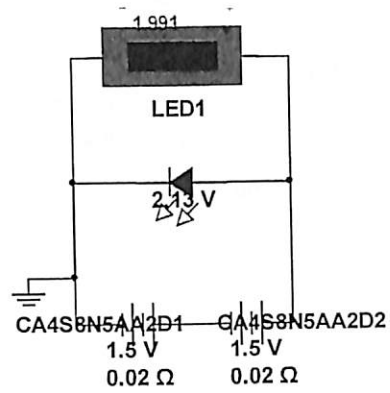


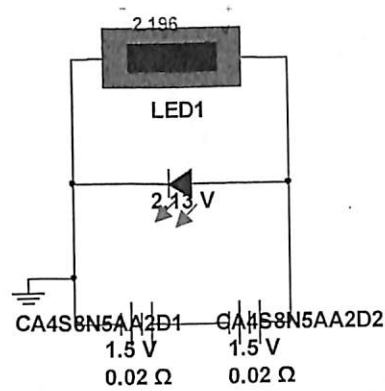
Figure 3.22: The $\text{Zn}+\text{ZnSO}_4 \cdot 7\text{H}_2\text{O} \parallel \text{CA67S8N5A} \parallel \text{MnO}_2$ coin cells open circuit potential with green LED.

The virtual analysis is important in order to compare with actual application of proton batteries (Figure 3.23). All the parameters configured in virtual analysis were selected based on OCV, discharge and $I-V$ analyses. The OCP values (1.5 V), r (0.02 Ω), and discharge capacity (26.7 mAh). The circuit was simulated and analyzed virtually via transient analysis of MULTISIM, as illustrated in Figure 3.24-3.25. Both of actual and virtual analyses confirmed the proton batteries were functional in both simulation and actual applications.

(a)



(b)



(c)

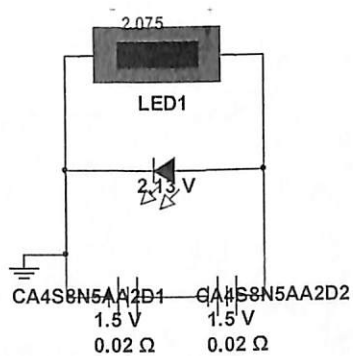


Figure 3.23: Simulation of $\text{Zn}+\text{ZnSO}_4 \cdot 7\text{H}_2\text{O} \parallel \text{CA67S8N5A} \parallel \text{MnO}_2$ coin cells using MULTISM (a) circuit components including virtual coin cells and LED, (b) during switch on and (c) after switch off.

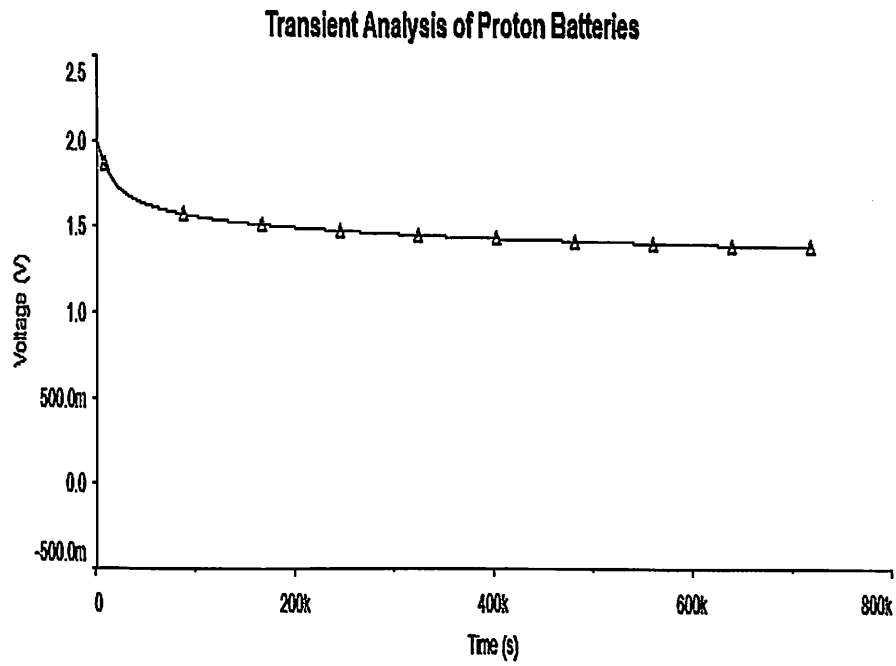


Figure 3.24: Transient analysis of $\text{Zn} + \text{ZnSO}_4 \cdot 7\text{H}_2\text{O} \parallel \text{CA67S8N5A} \parallel \text{MnO}_2$ coin cells using MULTISM.

CHAPTER 4

CONCLUSION AND SUGGESTION

5.0 Conclusion

In this study, the porous chitosan acetate-silica membranes have been successfully prepared using inverse porogen/polymer solubility technique. The optimum chitosan to silica ratio for producing largest macroporous membrane was 1:4. The optimum average pore size and degree of crystallinity of 5.9 μm and 90%, respectively were obtained. Fourier transform infrared analysis showed the interaction between chitosan, acetic acid and silica have been occurred based on the shifting of several functional group peaks intensity. The melting point of the membrane obtained from differential scanning calorimetry was 130°C. Thermogravimetry analysis shows the decomposition of the total of the membrane begins at a temperature of 200°C.

The membrane had the higher conductivity of $(4.7 \pm 1.1) \times 10^{-2} \text{ S cm}^{-1}$ after two-day immersion in 5.0 M ammonium acetate electrolyte solution compared with the membrane before immersed in ammonium acetate electrolyte $(6.0 \pm 0.1) \times 10^{-8} \text{ S cm}^{-1}$. The activation energy for membranes before and after immersed in 5.0 M ammonium acetate electrolyte solution were 0.2 and 0.03 eV, respectively. The breakdown voltage and window stability obtained from linear sweep voltammetry and cyclic voltammetry were 1.5 and 1.8 V, respectively.

The proton batteries displayed an open circuit potential of 1.5 V for 8 days and turned on LED for 40 hours. The internal current resistance of batteries was 0.02 Ω and maximum power density of 11.0 mW cm^{-2} . The specific discharge capacities of

proton batteries were 6.4, 10.7, 35.6 and 53.3 mA h g⁻¹ for 0.1, 0.2, 0.5 and 1.0 mA discharge current, respectively.

5.1 Suggestion

It suggested that future research work should focus on producing porous chitosan membrane using other simple technique such as ultrasonicator. This is because this technique will reduce the duration of sample preparation besides can produce uniform pore size and shape.

Other kind of salt such as ammonium nitrate, ammonium bromide can be used to replace ammonium acetate. Different kind of salts can give various results in term of electrochemical properties. Besides that, all the electrochemical properties can be investigated at high temperature. The analysis of fabricated proton batteries can be focus on elevated temperatures to find the resistance of batteries besides focus on failure analysis of batteries.

REFERENCES

- Al-Kahlout, A., Vieira, D., Avellaneda, C., Leite, E., Aegerter, M. and Pawlicka, A. (2009). *Gelatin-based protonic electrolyte for electrochromic windows*. *Ionics*, 16, pp. 13-19.
- Beck, F. and Rüetschi, P. (2000). *Rechargeable batteries with aqueous electrolytes*. *Electrochimica Acta*, 45, pp. 2467-2482.
- Bie, P., Liu, P., Yu, L., Li, X., Chen, L. and Xie, F. (2013). *The properties of antimicrobial films derived from poly(lactic acid)/starch/chitosan blended matrix*. *Carbohydrate Polymers*, 98, pp. 959-966.
- Bu, X., Zhou, Y., He, M., Chen, Z. and Zhang, T. (2014). *Optically active SiO₂/TiO₂/polyacetylene multilayered nanospheres: Preparation, characterization, and application for low infrared emissivity*. *Applied Surface Science*, 288, pp. 444-451.
- Chang, K.-S., Wang, H.-C. and Chung, T.-W. (2004). *Effect of regeneration conditions on the adsorption dehumidification process in packed silica gel beds*. *Applied Thermal Engineering*, 24, pp. 735-742.
- Chang, R. (1998). *Chemical Kinetics Chemistry*. WCB McGraw-Hill, United States of America, pp. 528-530.
- Clasen, C., Wilhelms, T. and Kulicke, W.-M. (2006). *Formation and characterization of chitosan membranes*. *Biomacromolecules*, 7, pp. 3210-3222.
- Du, J. F., Bai, Y., Pan, D. A., Chu, W. Y. and Qiao, L. J. (2009). *Characteristics of proton conducting polymer electrolyte based on chitosan acetate complexed with CH₃COONH₄*. *Journal of Polymer Science Part B: Polymer Physics*, 47, pp. 549-554.
- Enescu, D., Hamciuc, V., Ardeleanu, R., Cristea, M., Ioanid, A., Harabagiu, V. and Simionescu, B. C. (2009). *Polydimethylsiloxane modified chitosan. Part III: Preparation and characterization of hybrid membranes*. *Carbohydrate Polymers*, 76, pp. 268-278.
- Gray, F. M. (1997). *Polymer electrolytes*. The Royal Society of Chemistry, Information Services, Cambridge.
- Kim, K. M., Park, N.-G., Ryu, K. S. and Chang, S. H. (2002). *Characterization of poly(vinylidene fluoride-co-hexafluoropropylene)-based polymer electrolyte filled with TiO₂ nanoparticles*. *Polymer*, 43, pp. 3951-3957.

- Kim, K. M., Park, N.-G., Ryu, K. S. and Chang, S. H. (2006). *Physical and electrochemical characterizations of poly(vinylidene fluoride-co-hexafluoropropylene)/SiO₂-based polymer electrolytes prepared by the phase-inversion technique*. Journal of Applied Polymer Science, 102, pp. 140-148.
- Kim, K. M., Ryu, K. S., Kang, S. G., Chang, S. H. and Chung, I. J. (2001). *The effect of silica addition on the properties of poly((vinylidene fluoride)-co-hexafluoropropylene)-based polymer electrolytes*. Macromolecular Chemistry and Physics, 202, pp. 866-872.
- Koh, J., Ahmad, Z. A. and Mohamad, A. A. (2011). *Bacto agar-based gel polymer electrolyte*. Ionics, pp. 1-6.
- Li, Z., Liu, H., Liu, Y., He, P., Li, J., Zheng, L. and Li, J. (2005). *Effect of methylsilsesquioxane filler on the properties of ionic liquid based polymer electrolyte*. Polymer, 46, pp. 7578-7584.
- Linden, D. (2002). *Basics Concepts*. In Reddy, T. B. (ed) Handbook of Batteries. McGraw-Hill, pp. 1.9-1.10.
- Liu, Y., Lee, J. Y. and Hong, L. (2003). *Morphology, crystallinity, and electrochemical properties of in situ formed poly (ethylene oxide)/TiO₂ nanocomposite polymer electrolytes*. Journal of Applied Polymer Science, 89, pp. 2815-2822.
- Matet, M., Heuzey, M.-C., Pollet, E., Ajjji, A. and Avérous, L. (2013). *Innovative thermoplastic chitosan obtained by thermo-mechanical mixing with polyol plasticizers*. Carbohydrate Polymers, 95, pp. 241-251.
- Mei, L., Hu, D., Ma, J., Wang, X., Yang, Y. and Liu, J. (2012). *Preparation, characterization and evaluation of chitosan macroporous for potential application in skin tissue engineering*. International Journal of Biological Macromolecules, pp.
- Ng, L. S. and Mohamad, A. A. (2006). *Protonic battery based on a plasticized chitosan-NH₄NO₃ solid polymer electrolyte*. J. Power Sources, 163, pp. 382-385.
- Ng, L. S. and Mohamad, A. A. (2008). *Effect of temperature on the performance of proton batteries based on chitosan-NH₄NO₃-EC membrane*. Journal of Membrane Science, 325, pp. 653-657.
- Pattnaik, S., Nethala, S., Tripathi, A., Saravanan, S., Moorthi, A. and Selvamurugan, N. (2011). *Chitosan scaffolds containing silicon dioxide and zirconia nano particles for bone tissue engineering*. International Journal of Biological Macromolecules, 49, pp. 1167-1172.
- Pratap, R., Singh, B. and Chandra, S. (2006). *Polymeric rechargeable solid-state proton battery*. Journal of Power Sources, 161, pp. 702-706.

- Rajendran, S. and Uma, T. (2000). *Lithium ion conduction in PVC-LiBF₄ electrolytes gelled with PMMA*. Journal of Power Sources, 88, pp. 282-285.
- Ramesh, S. and Liew, C.-W. (2012). *Exploration on nano-composite fumed silica-based composite polymer electrolytes with doping of ionic liquid*. Journal of Non-Crystalline Solids, 358, pp. 931-940.
- Santos, D. E. S., Neto, C. G. T., Fonseca, J. L. C. and Pereira, M. R. (2008). *Chitosan macroporous asymmetric membranes-Preparation, characterization and transport of drugs*. J. Membr. Sci., 325, pp. 362-370.
- Shirosaki, Y., Tsuru, K., Hayakawa, S., Osaka, A., Lopes, M. A., Santos, J. D. and Fernandes, M. H. (2005). *In vitro cytocompatibility of MG63 cells on chitosan-organosiloxane hybrid membranes*. Biomaterials, 26, pp. 485-493.
- Tolchard, J. (2009). *ELECTROLYTES | Solid: Protons*. In Editor-in-Chief: Jürgen, G. (ed) Encyclopedia of Electrochemical Power Sources. Elsevier, Amsterdam, pp. 188-195.
- Tran, C. D., Duri, S., Delneri, A. and Franko, M. (2013). *Chitosan-cellulose composite materials: Preparation, Characterization and application for removal of microcystin*. Journal of Hazardous Materials, 252-253, pp. 355-366.
- Vallet-Regi, M., Ruiz-Gonzalez, L., Izquierdo-Barba, I. and Gonzalez-Calbet, J. M. (2006). *Revisiting silica based ordered mesoporous materials: medical applications*. Journal of Materials Chemistry, 16, pp. 26-31.
- Vincent, C. and Scrosati, B. (1997). *Modern Batteries 2nd Edition*. Elsevier.
- Wang, F., Yang, J. and Wu, K. (2009). *Mesoporous silica-based electrochemical sensor for sensitive determination of environmental hormone bisphenol A*. Analytica chimica acta, 638, pp. 23-28.
- Weast, R. C. (1977). *CRC Handbook of Chemistry and Physics: A Ready-Reference Book of Chemical and Physical Data*. CRC Press.
- Yap, S. C. and Mohamad, A. A. (2007). *Proton Batteries with Hydroponics Gel as Gel Polymer Electrolyte*. Electrochemical and Solid-State Letters, 10, pp. A139-A141.
- Zeng, X. and Ruckenstein, E. (1996). *Control of Pore Sizes in Macroporous Chitosan and Chitin Membranes*. Ind. Eng. Chem. Res., 35, pp. 4169-4175.

LIST OF PUBLICATIONS

Articles

1. Alias, N. and Mohamad, A. A. *Morphology study of electrodeposited zinc from zinc sulfate solutions as anode for zinc-air and zinc-carbon batteries*. Journal of King Saud University - Engineering Sciences (Article in press).
2. Masri, M. N., Nazeri, M. F. M., Ng, C. Y. and Mohamad, A. A. *Tapioca binder for porous zinc anodes electrode in zinc-air batteries*. Journal of King Saud University - Engineering Sciences (Article in press).
3. Siti Salwa Alias, Siew Mian Chee, A.A. Mohamad. *Chitosan-ammonium acetate-ethylene carbonate Membrane for Proton Batteries*, Arabian Journal of Chemistry, 2014 minor correction.

Book

1. Siti Salwa Alias, Ahmad Azmin Mohamad. *Synthesis of Zinc Oxide by Sol-Gel Method for Photoelectrochemical Cell*, SpringerBriefs in Materials (2014).

Conference Proceeding

1. S. S. Alias and A. A. Mohamad. *Preparation and Characterization of Porous Chitosan Membrane for Proton Battery*. Proceeding International Conference on Materials for Advanced Technologies (ICMAT 2013), page 34.
2. Siti Salwa Alias, Zulkifli Mohamad Ariff, and Ahmad Azmin Mohamad. *Preparation and Characterization of Porous Silica-Chitosan Membrane for Proton Batteries*. Proceeding Asia-Pacific Conference on Electrochemical Energy Storage and Conversion (APEnergy2014).

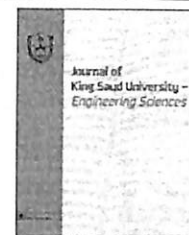
APPENDIXES



King Saud University

Journal of King Saud University – Engineering Sciences

www.ksu.edu.sa
www.sciencedirect.com



ORIGINAL ARTICLE

Morphology study of electrodeposited zinc from zinc sulfate solutions as anode for zinc-air and zinc-carbon batteries

Nurhaswani Alias, Ahmad Azmin Mohamad *

School of Materials and Mineral Resources Engineering, Universiti Sains Malaysia, 14300 Nibong Tebal, Penang, Malaysia

Received 21 February 2013; accepted 12 March 2013

KEYWORDS

Zn deposition;
Copper substrate;
Current density;
Zinc-air battery;
Zinc-carbon battery

Abstract The morphology of Zinc (Zn) deposits was investigated as anode for aqueous batteries. The Zn was deposited from zinc sulfate solution in direct current conditions on a copper surface at different current densities. The morphology characterization of Zn deposits was performed via field emission scanning electron microscopy. The Zn deposits transformed from a dense and compact structure to dendritic form with increasing current density. The electrodeposition of Zn with a current density of 0.02 A cm^{-2} exhibited good morphology with a high charge efficiency that reached up to 95.2%. The Zn deposits were applied as the anode in zinc-air and zinc-carbon batteries, which gave specific discharge capacities of 460 and 300 mA h g^{-1} , respectively.

© 2013 Production and hosting by Elsevier B.V. on behalf of King Saud University.

1. Introduction

Zinc (Zn) is a promising anode candidate for secondary alkaline batteries because of its abundance, relatively low cost, compatibility with aqueous electrolytes, and low-toxic element (Hilder et al., 2012). In secondary alkaline batteries, the anode should be efficient as a reducing agent and must have a high coulombic output, good conductivity, ease of fabrication, and low cost (Linden, 2001). The applications of Zn as an anode tremendously increased because Zn possesses these favor-

able properties. Furthermore, Zn has a large overpotential for hydrogen gas evolution, which allows Zn to operate at lower potentials than the window stability of water (Abe and Miyazaki, 2012). A Zn anode is generally fabricated by various methods such as electrodeposition (Gomes and da Silva Pereira, 2006; Popov et al., 1978) and paste drying (Masri and Mohamad, 2009).

Recent investigations have highlighted electrodeposition as an attractive approach that not only provides a cost-effective intensive method that does not require any equipment, but also has the advantage to control the shape and grain size of the deposit and can provide a high surface area (Bunshah, 1994; Leung et al., 2011; Lehr and Saidman, 2012). Bicelli et al. (2008) also reported that interdiffusion or chemical reactions can be minimized using a low processing temperature (room temperature) during the electrodeposition process. Therefore, various studies on the electrodeposition of Zn were performed in different operating conditions to improve the

* Corresponding author. Tel.: +60 4599 6118; fax: +60 4594 1011.
E-mail address: azmin@eng.usm.my (A.A. Mohamad).

Peer review under responsibility of King Saud University.



Production and hosting by Elsevier



ORIGINAL ARTICLE

Tapioca binder for porous zinc anodes electrode in zinc–air batteries

Mohamad Najmi Masri, Muhammad Firdaus Mohd Nazeri, Chai Yan Ng, Ahmad Azmin Mohamad *

School of Materials and Mineral Resources Engineering, Universiti Sains Malaysia, 14300 Nibong Tebal, Penang, Malaysia

Received 25 March 2013; accepted 3 June 2013

KEYWORDS

Tapioca;
Binder;
Porous zinc anode;
Zinc-air battery

Abstract Tapioca was used as a binder for porous Zn anodes in an electrochemical zinc-air (Zn-air) battery system. The tapioca binder concentrations varied to find the optimum composition. The effect of the discharge rate at 100 mA on the constant current, current–potential and current density–power density of the Zn-air battery was measured and analyzed. At concentrations of 60–80 mg cm⁻³, the tapioca binder exhibited the optimum discharge capability, with a specific capacity of approximately 500 mA h g⁻¹ and a power density of 17 mW cm⁻². A morphological analysis proved that at this concentration, the binder is able to provide excellent binding between the Zn powders. Moreover, the structure of Zn as the active material was not affected by the addition of tapioca as the binder, as shown by the X-ray diffraction analysis. Furthermore, the conversion of Zn into ZnO represents the full utilization of the active material, which is a good indication that tapioca can be used as the binder.

© 2013 Production and hosting by Elsevier B.V. on behalf of King Saud University.

1. Introduction

Tapioca is a common plant that can be found in almost every tropical country. Its biodegradable starch is an important source of carbohydrates (Atichokudomchai and Varavinit, 2003; Blagbrough et al., 2010; Breuninger et al., 2009). In general, the starch of tapioca is made up of two major macromolecular components, which can be identified as amylose and

amylopectin (Breuninger et al., 2009; Chung and Liu, 2009; Pérez et al., 2009). Amylose is a linear component polymer that is primarily composed of (1 → 4)-linked α -glucan (Fig. 1a). The degree of polymerization of this polymer can be as high as 600. In tapioca starch, the amylose content can vary from 17% to 20%. Alternatively, amylopectin is the major component of tapioca starch (Fig. 1b). This polymer is made up of α (1 → 4)-linked α -glucan with an α -(1 → 6) branch point. Amylopectin is significantly different than amylose because amylopectin contains approximately 5% branch points (Chung and Liu, 2009; Pérez et al., 2009).

When tapioca starch is heated in excess water, an irreversible structure transition takes place, which is known as starch gelatinization or pasting. The granules of tapioca starch lose their birefringence and crystallinity as more water is absorbed. Upon cooling, tapioca starch experiences an increase in

* Corresponding author. Tel.: +60 4599 6118; fax: +60 4594 1011.
E-mail address: azmin@eng.usm.my (A.A. Mohamad).

Peer review under responsibility of King Saud University.



Production and hosting by Elsevier

The Zn–air battery clearly had better performance with a high discharge capacity compared with the Zn–carbon battery even when similar Zn deposit samples were used as anode for both systems. This result is due to the fact that the Zn–air battery directly used oxygen from the atmosphere, which results in unlimited capacity and high energy density.

4. Conclusions

Zn was successfully deposited via the direct current electrodeposition process in ZnSO_4 solution without the presence of additives. Electrodeposition of pure Zn at a current density of 0.02 A cm^{-2} produced fine morphology with a high current efficiency without the presence of dendrites. Electrochemical results show that the Zn deposits achieved good specific capacity and stability during the discharge process for the Zn–air and Zn–carbon battery systems. Therefore, a good morphology of Zn deposits can be applied as anode materials in aqueous battery cells.

Acknowledgment

The authors would like to thank MN Masri for the experimental help and ERGS Grant No 203/PBAHAN/6730006 for the financial support in this study.

References

- Abe, T. and Miyazaki, K., 2012, (Invited) Aqueous Electrolyte-Based Metal–Air Batteries: Challenges for Rechargeable Zinc Electrodes and Reversible Air Electrodes. Meeting Abstracts, 2012. The Electrochemical Society, p. 1182.
- Baik, D.S., Fray, D.J., 2001. Electrodeposition of zinc from high acid zinc chloride solutions. *J. Appl. Electrochem.* 31, 1141–1147.
- Bicelli, L.P., Bozzini, B., Mele, C., D'urzo, L., 2008. A review of nanostructural aspects of metal electrodeposition. *Int. J. Electrochem. Sci.* 3, 356–408.
- Bunshah, R.F., 1994. Handbook of Deposition Technologies for Films and Coatings – Science, Second ed.. Technology and Applications William Andrew Publishing, Noyes.
- Chu, M.G., Mcbreen, J., Adzic, G., 1981. Substrate effects on zinc deposition from zincate solutions. *J. Electrochem. Soc.* 128, 2281–2286.
- Freitas, M.B.J.G., De Pietre, M.K., 2005. Deposit morphology of the zinc recovery by electrodeposition from the spent Zn– MnO_2 batteries. *J. Power Sources* 143, 270–274.
- Gomes, A., Da Silva Pereira, M.I., 2006. Pulsed electrodeposition of Zn in the presence of surfactants. *Electrochim. Acta* 51, 1342–1350.
- Hamlén, R.P., Atwater, T.B., 2001. Metal/Air Batteries Handbook of Batteries. D. Linden, T. B. Reddy, New York.
- Hilder, M., Winther-Jensen, B., Clark, N.B., 2012. The effect of binder and electrolyte on the performance of thin zinc–air battery. *Electrochim. Acta* 69, 308–314.
- Koh, J.C.H., Ahmad, Z.A., Mohamad, A.A., 2011. Self-aligned TiO_2 nanotube arrays produced by air–cathode as electrode. *J. Alloys Compd.* 509, 8707–8715.
- Lehr, I.L., Saidman, S.B., 2012. Influence of sodium bis(2-ethylhexyl) sulfosuccinate (AOT) on zinc electrodeposition. *Appl. Surf. Sci.* 258, 4417–4423.
- Leung, P.K., Ponce-De-Leon, C., Low, C.T.J., Walsh, F.C., 2011. Zinc deposition and dissolution in methanesulfonic acid onto a carbon composite electrode as the negative electrode reactions in a hybrid redox flow battery. *Electrochim. Acta* 56, 6536–6546.
- Li, G.-R., Dawa, C.-R., Bu, Q., Lu, X.-H., Ke, Z.-H., Hong, H.-E., Zheng, F.-L., Yao, C.-Z., Liu, G.-K., Tong, Y.-X., 2007. Electrochemical self-assembly of ZnO nanoporous structures. *J. Phys. Chem. C* 111, 1919–1923.
- Linden, D., 2001. Basic concepts. In: Linden, D., Reddy, T.B. (Eds.), Handbook of Batteries. McGraw Hill, New York.
- Lou, H.H., Huang, Y., 2006. Electroplating. In Encyclopedia of Chemical Processing. Taylor & Francis.
- Masri, M.N., Mohamad, A.A., 2009. Effect of adding potassium hydroxide to an agar binder for use as the anode in Zn–air batteries. *Corrosion Sci.* 51, 3025–3029.
- Popov, K.I., Keca, D.N., Andelic, M.D., 1978. Electrodeposition of zinc on copper from alkaline zincate solutions. *J. Appl. Electrochem.*, 19–23.
- Shaigan, N., Qu, W., Takeda, T., 2010. Morphology Control of Electrodeposited Zinc from Alkaline Zincate Solutions for Rechargeable Zinc Air Batteries. *J. Electrochem. Soc.* 28, 35–44.
- Sharifi, B., Mojtahedi, M., Goodarzi, M., Khaki, J.V., 2009. Effect of alkaline electrolysis conditions on current efficiency and morphology of zinc powder. *Hydrometallurgy* 99, 72–76.

Ms. Ref. No.: ARABJC-D-13-00869

Title: Chitosan-ammonium acetate-ethylene carbonate Membrane for Proton Batteries

Arabian Journal of Chemistry

Chitosan-ammonium acetate-ethylene carbonate Membrane for Proton Batteries

Siti Salwa Alias, Siew Mian Chee and Ahmad Azmin Mohamad*

School of Materials and Mineral Resources Engineering

Universiti Sains Malaysia, 14300 Nibong Tebal, Penang, Malaysia

*Corresponding author: azmin@eng.usm.my

Tel: +60 4599 6118; Fax: +60 4594 1011

Chitosan-ammonium acetate-ethylene carbonate Membrane for Proton Batteries

Siti Salwa Alias, Siew Mian Chee and Ahmad Azmin Mohamad*

School of Materials and Mineral Resources Engineering

Universiti Sains Malaysia, 14300 Nibong Tebal, Penang, Malaysia

*Corresponding author: azmin@eng.usm.my

Tel: +60 4599 6118; Fax: +60 4594 1011

Abstract

Proton-conducting membranes were prepared using solution-casting technique. The highest membrane conductivity of $(3.83 \pm 0.73) \times 10^{-3} \text{ S cm}^{-1}$ was achieved in chitosan acetate-50 wt.% ammonium acetate-70 wt.% ethylene carbonate. The batteries were fabricated with a configuration of $\text{Zn}+\text{ZnSO}_4 \cdot 7\text{H}_2\text{O} \parallel$ chitosan membrane $\parallel \text{MnO}_2$ and $\text{Zn}+\text{ZnSO}_4 \cdot 7\text{H}_2\text{O} \parallel$ chitosan membrane $\parallel \text{V}_2\text{O}_5$. The cathode materials produced open circuit voltages of 1.60 and 1.27 V using manganese (IV) oxide (MnO_2) and vanadium (IV) oxide (V_2O_5), respectively. The discharge capacities of the batteries were 45.0 and 34.7 mAh using MnO_2 and V_2O_5 cathode at 1.0 mA, respectively. The maximum power densities were 1.83 mW cm^{-2} for the battery with MnO_2 and 1.36 mW cm^{-2} for the battery with V_2O_5 cathode.

Keywords: Proton-conducting membrane; Chitosan; Cathode; V_2O_5 ; MnO_2 ; Proton batteries

SPRINGER BRIEFS IN MATERIALS

Siti Salwa Alias
Ahmad Azmin Mohamad

Synthesis of Zinc Oxide by Sol– Gel Method for Photoelectro- chemical Cells

 Springer

Acknowledgments

The authors would like to thank the School of Materials and Minerals Resources Engineering, Universiti Sains Malaysia, and its staff for providing good research facilities and valuable scientific knowledge. We also thank all members of the Battery Research Group for their support and valuable scientific discussions, especially to Li Jian Khoo and Ann Ling Tan for their contribution to the experiments. We would also like to thank Exploratory Research Grant Scheme, ERGS (203/PBAHAN/6730006) for the financial support of this work.

Siti Salwa Alias
Ahmad Azmin Mohamad

ICMAT 2013

7TH INTERNATIONAL CONFERENCE ON
MATERIALS FOR ADVANCED TECHNOLOGIES

30 JUNE - 5 JULY, SUNTEC SINGAPORE

TECHNICAL PROGRAMME

WWW.MRS.ORG.SG

Organised By

MRS
Materials Research Society
SINGAPORE



In Association With



- Sn. 16 A-PO1-16
Spin-state Effect of Iron Active Sites in Fe-based Catalysts for Oxygen Reduction Reaction from Molecular Orbital Theory
Jangsoo LEE^{1*}, Jung Hee YOON², Jaephil CHO^{1*}
¹Interdisciplinary School of Green Energy, Ulsan National Institute of Science and Technology (UNIST), South Korea, ²Ulsan National Institute of Science and Technology (UNIST), South Korea
- Sn. 17 A-PO1-17
Studies Illustrating on the Properties Enhancement of the Acrylate-based Polymer Electrolyte Membranes
R. Shanti RAJANTHARAN^{1*}, Ramesh SUBRAMANIAM¹, Ramesh KASI¹
¹Department of Physics, University of Malaya, Malaysia
- Sn. 18 A-PO1-18
Synthesis and Characterization of TiO₂/c by a Simple Thermal Decomposition Method
Lilong XIONG^{1*}, Youlong XU^{1*}, Tao TAO¹, Pei LEI¹
¹Electronic Materials Research Laboratory, Key Laboratory of the Ministry of Education & International Center of Dielectric Research, Xi'an Jiaotong University, China
- Sn. 19 A-PO1-19
Composite Grown from Emulsion Explosive
Xinghua XIE^{1*}
¹Anhui University of Science and Technology, China
- Sn. 20 A-PO1-20
Li-cycling Studies of Nanostructured Co₃O₄, CoO and CoN and Investigating Their Use as Anodes for Li-ion Batteries
Prithvi GUNDLAPALLI^{1,2*}, M. V. REDDY^{3*}, B.V.R. CHOWDARI¹, Kian Ping LOH¹
¹National University of Singapore, Singapore, ²St Andrew's Junior College, Singapore, ³Department of Physics, Solid State Ionics/Advanced Batteries Lab, Singapore
- Sn. 21 A-PO1-21
Flexible Graphene Composites for Energy Storage Applications
Ce Yao FOO^{1*}, Afriyanti SUMBOJA¹, Pooi See LEE^{2*}
¹Nanyang Technological University, Singapore, ²Temasek Laboratories, Nanyang Technological University, Singapore
- Sn. 22 A-PO1-22
Study of Storage Capacity in Various Graphene Based Solid State Supercapacitors
Subramaniam CHITTUR KRISHNASWAMY^{1*}, Boopalan GANAPATHY²
¹Material Physics Division, School of Advanced Sciences, Vellore Institute of Technology, India, ²School of Electronics Engineering, VIT University, India
- Sn. 23 A-PO1-23
Preparation and Characterization of Porous Chitosan Membrane for Proton Battery
Siti ALIAS^{1*}, Ahmad Azmin MOHAMAD^{1*}
¹School Of Materials and Mineral Resources Engineering, Universiti Sains Malaysia, Malaysia
- Sn. 24 A-PO1-24
Optimized 4V Spinel Cathode Materials with High Energy and High Pellet Density for Li-ion Cells
Sanghan LEE^{1*}, Jaephil CHO^{2*}
¹Ulsan National Institute of Science and Technology (UNIST), South Korea, ²Interdisciplinary School of Green Energy, Ulsan National Institute of Science and Technology (UNIST), South Korea
- Sn. 25 A-PO1-25
Electrochemical Performance of Li[Ni_{0.33}Co_{0.33}Mn_{0.33}]O₂ Cathode Compositing with Ketjen Black
Yong Joon PARK^{1*}, Chang Su KIM¹
¹Advanced Materials Engineering, Kyonggi University, South Korea
- Sn. 26 A-PO1-26
CNF/Co₃O₄ Composite for Enhanced Lithium Air Batteries
Yong Joon PARK^{1*}, Daesik KIM², Seuk Buom KIM²
¹Advanced Materials Engineering, Kyonggi University, South Korea, ²Kyonggi University, South Korea
- Sn. 27 A-PO1-27
Facile Preparation and Adjustable Thermal Properties of Stearic-acid/graphene-oxide Shape-stabilized Phase-change Composites
Benxia LI^{1*}, Jianfang WANG^{2*}
¹Department of Materials Science and Engineering, Anhui University of Science and Technology, China, ²Department of Physics, The Chinese University of Hong Kong, Hong Kong SAR
- Sn. 28 A-PO1-28
Na₂Ti₆O₁₃: A Potential Anode Material for Grid Storage Sodium-ion Batteries
Ashish RUDOLA^{1*}, Saravanan KUPPAN², Palani BALAYA²
¹Mechanical Engineering, National University of Singapore, Singapore, ²National University of Singapore, Singapore
- Sn. 29 A-PO1-29
The Effect of Materials Synthesis Conditions on Oxygen Non-stoichiometry and Interlayer Mixing in Layered Rock Salt Cathode Materials for Lithium Ion Batteries
Soon Peng SOO^{1*}, Mohd Sobri IDRIS¹, Azmi RAHMAT¹, Rozana Aina MAULAT OSMAN¹, Shamsul Baharin JAMALUDIN¹, Zul Azhar ZAHID JAMAL¹
¹Sustainable Engineering Research Cluster, School of Materials Engineering, University Malaysia Perlis, Malaysia
- Sn. 30 A-PO1-30
3D Interconnected Nanoporous Nickel for Electrochemical Capacitors
Xing HU^{1*}, JianLong JIANG¹, Zhiyuan LING¹
¹South China University of Technology, China
- Sn. 31 A-PO1-31
Study of Si Based Electrode Stability with Dilatometry
Ming ZHAO^{1*}, Denis Y.W. YU^{2,3*}
¹TUM CREATE, Singapore, ²Energy Research Institute @ Nanyang Technological University (ERI @ NTU), Singapore, ³School of Energy and Environment, City University of Hong Kong, Hong Kong SAR
- Sn. 32 A-PO1-32
Diffusion of Metal Atoms in Bulk and Nanostructured Si
Oleksandr MALYI^{1*}, Fleur LEGRAIN¹, Teck TAN², Sergei MANZHOS³
¹Department of Mechanical Engineering, National University of Singapore, Singapore, ²Institute of High Performance Computing, Singapore, ³National University of Singapore, Singapore
- Sn. 33 A-PO1-33
Capacitance and Adhesion of Hydrous Ruthenium Oxides Prepared on Tantalum Electrodes by Thermolysis Method
Jie WANG^{1*}, Youlong XU¹
¹Xi'an Jiaotong University, China

ICMAT13-A-1275 (Symposium A: Advanced Energy Storage Systems: Lithium ion batteries and beyond)

**Preparation and Characterization of Porous Chitosan Membrane for Proton
Battery**

S. S. Alias and *A. A. Mohamad

Abstract

The porous chitosan membrane has been prepared by using the ultrasonic and solution-cast technique. The chitosan acetate membrane is mixed with various amount of silica from 17-80 wt. %. All the membrane has been immersed in 8 M sodium hydroxide at 60 °C for 1 day to produce porous chitosan acetate-silica membrane. The porous chitosan acetate membrane contain with 67 wt. % silica had the highest pores size of 8.47 μm . This membrane had the highest conductivity of $(8.61 \pm 1.44) \times 10^{-4} \text{ S cm}^{-1}$ after immersed in 5 M ammonium acetate salt solution for two days. The battery has been fabricated with a configuration of $\text{Zn} + \text{ZnSO}_4 \cdot 7\text{H}_2\text{O} \parallel \text{chitosan acetate-67 wt. \% silica-5 M ammonium acetate electrolyte} \parallel \text{MnO}_2$ gave the open circuit voltage of 1.60 V and can sustain up to 8 days.

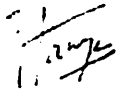
Keywords: Porous chitosan; Membrane; Silica; Ammonium acetate; Proton batteries

*Corresponding author. Tel: +604599 6118; Fax: +6045941011
E-mail address: azmin@eng.usm.my (A.A. Mohamad)

Looking forward to meeting you and wish you a productive and successful workshop
in MSI, UniKL

Thank you for your consideration and cooperation.

Yours faithfully,



Nor Haniza Binti Bakhtiar Jemily

Lecturer,

UniKL MSI,

Kulim Hi-Tech,

09000 Kulim, Kedah

Tel: 604 403 5199/200; Fax: 604 403 5201

Emails: norhaniza@msi.unikl.edu.my



UNIVERSITI KUALA LUMPUR
MALAYSIAN SPANISH INSTITUTE
Lot 13-16, Kulim Hi-Tech Park
09000 Kulim, Kedah Darul Aman
Malaysia
Tel: (604) 4035199/4035200
Fax: (604) 4035201
Website: www.unikl.edu.my

Nor Haniza Binti Bakhtiar Jemily,
Mechanical Section,
UniKL MSI,
Kulim Hi-Tech,
09000 Kulim,
Kedah.

Assoc. Prof. Dr. Ahmad Azmin Mohamad,
School of Materials & Mineral Resources Engineering,
Universiti Sains Malaysia,
14300 Nibong Tebal, Penang, Malaysia.

12 November 2013

Dear Professor,

Invitation for Mendeley and EndNote Workshop

On behalf of Universiti Kuala Lumpur Malaysia Spanish Institute (UniKL MSI) we would like to invite you as a speaker for the workshop on Mendeley and EndNote.

Details are as follows:

Date : 20th November 2013

Time : 8 am to 5 pm.

Venue : Al-Farabi Meeting Room

The participants for this workshop will involves 30 lecturers from UniKL MSI. It would be a great pleasure if you accept this invitation and reply to me at your earliest convenience.

Please do not hesitate to contact me who will ensure you are set up with the facilities and assistance needed.

Preparation and Characterization of Porous Silica-Chitosan Membrane for Proton Batteries

Siti Salwa Alias, Zulkifli Mohamad Ariff, and Ahmad Azmin Mohamad*

School of Materials and Mineral Resources Engineering

Universiti Sains Malaysia, 14300 Nibong Tebal, Penang, Malaysia

**Corresponding author Tel: +604599 6118; Fax: +6045941011*

**Email: azmin@eng.usm.my*

Abstract

Porous chitosan membranes were prepared by stirring mixed solution-cast method. Different concentration of sodium hydroxide porogen removal solution was used to dissolve silica from chitosan acetate membrane. The morphology and structural properties were determined using FESEM and XRD. The optimum average pore size and degree of crystallinity of 5.9 μm and 90%, respectively were obtained. The chemical interactions of membranes were detected using FTIR. The membrane exhibited its highest conductivity at $(4.7 \pm 1.1) \times 10^{-3} \text{ S cm}^{-1}$ after two days immersion in 5.0 M $\text{NH}_4\text{CH}_3\text{COO}$ electrolyte solution. The membrane had good electrochemical properties based on cyclic voltametry. Fabricated proton batteries displayed an open circuit potential of 1.4 V for 6 days. The specific discharge capacities of proton batteries was 12.0 mA h g^{-1} for 1.0 mA discharge current.

APEnergy 2014 Conference Book

February 5-8, 2014

INDIANIA CONVENTION AND EXHIBITION CENTRE, AUSTRALIA